Hindawi
Geofluids
Volume 2022, Article ID 5560387, 25 pages
https://doi.org/10.1155/2022/5560387

Research Article

Assessment of Chemical Effects on Wellbore Stability in Transition Shale Formation

Hai Lin,[1,2] Jingen Deng,[1] Chao Luo,[1] Lin Li,[3] and Hailong Liu[2]

[1]*State Key Laboratory of Petroleum Resources and Prospecting and College of Petroleum Engineering, China University of Petroleum, Beijing 102249, China*
[2]*State Key Laboratory of Offshore oil Exploitation, CNOOC China Limited, Tianjin Branch, Tianjin 300459, China*
[3]*Research Institute of Exploration and Development, Changqing Oilfield Company, Petro China, Xian, 710021 Shanxi, China*

Correspondence should be addressed to Jingen Deng; dengjingen@126.com

Received 21 January 2021; Accepted 23 March 2022; Published 20 April 2022

Academic Editor: Meng Meng

Substantial research has been conducted on the mechanisms responsible for the wellbore collapse in shale formations. For chemically active soft shale formations, pore pressure and stress change due to osmotic pressure and hydration swelling are usually recognized as the primary mechanisms, while for chemically inactive hard shale formation, wellbore instability is generally attributed to weak structural planes like bedding planes and microcracks. In this paper, experimental testing and analytical and numerical analyses are performed to reveal the dominant mechanism of the frequently encountered severe wellbore instability events in the middle-deep shale formation in the Bohai oil field of China. It is evidenced from the physical and chemical experimental testing that the middle-deep shale features both medium chemical activity and abundant bedding planes and microcracks, indicating that the middle-deep shale is in the transition process from chemically actively soft shale to the chemically inactive but laminated and fractured hard shale. Mechanical testing also shows considerable strength degradation of the middle-deep transition shale due to drilling fluid-shale interaction. Analysis through a hydro-chemo-mechanical coupling theory shows that the extent of the damage zone around the wellbore is limited if only pore pressure change and hydration swelling caused by the chemical difference between the drilling fluid and the formation fluid are considered, which cannot explain the severe wellbore collapse in the drilling process. In contrast, when pore pressure increase and strength degradation of the shale due to drilling fluid penetration along the bedding planes and microcracks are taken into account, a damage zone of 3~4 times of the wellbore diameter can be generated, implying that the dominant mechanism of the wellbore instability in the middle-deep transition shale formation should be the pore pressure change and strength degradation resulted from drilling fluid penetration along the bedding planes and microcracks.

1. Introduction

The wellbore instability is a worldwide technical problem in drilling engineering, and it is also one of the important issues of safe and efficient drilling. In recent years, wellbore collapse accidents in brittle shale formations have occurred frequently, and the problem of wellbore instability needs to be solved urgently.

According to their physical, chemical, and mechanical characteristics, shale can be divided into two major categories: one is characterized by low rolling recovery rate, strong pulping ability, and high cation exchange capacity (CEC), which is easy to swell [1]. Abundant studies have shown that the pore pressure and stress changes caused by osmotic pressure and hydration swelling [2] are the main mechanisms of this type of chemically active shale formation. The other type is characterized by the weak hydration swelling capacity and structural planes. However, the mechanism of wellbore instability in such brittle shale formations is still unclear.

Research on wellbore stability of shale has gone through several stages, such as pure mechanics research [3], drilling fluid chemistry research [4], mechanics-chemistry coupling research [5], and thermo-hydro-mechanical-chemical (T-H-M-C) [6] multifield coupling research. Related research

Figure 1: Shale sample from Bohai oil field.

Table 1: Mineral composition and content.

Sample	Mineral composition (%)					
	Quartz	Plagioclase	Calcite	Dolomite	Siderite	Clay mineral
1	22.8	12.8	9.5	14	1.9	39
2	19.7	8.7	8.8	12.6	19.7	30.5
3	44.9	23.5	0.0	5.9	3.9	21.8
4	41.6	10.6	1.3	3.7	0.9	41.9
5	34.3	7.4	0.6	7.2	0.9	49.6
6	39.2	9.3	0.4	5.1	0.8	45.2

Table 2: Clay minerals relative content.

Sample	Clay mineral content (%)				Interstratified ratio (%S)
	S	I/S	I	Kao	
1	—	71	18	4	15
2	—	71	17	—	15
3	—	61	39	—	15
4	—	72	17	4	20
5	—	78	15	3	20
6	—	81	12	3	20

on the stability of chemically active shale formation includes the following: (1) based on the stress study of porous elastic media, a model of stress around the wellbore was established after drilling, and the stress distribution around the wellbore of the inclined well was established taking into account the anisotropy of in situ stress [7]; the effect of drilling fluid on the mechanical properties of chemically active shale rock would reduce the strength of the shale [4]; (2) based on the theory of isotropic linear elasticity, a calculation method of stress distribution around the wellbore under the combined action of in situ stress and mud liquid pressure was established, which laid a theoretical foundation for the quantitative analysis of wellbore stability [8, 9]; (3) based on the study of the swelling of chemically active shale caused by different drilling fluids [10], the relationship between shale hydration swelling and strain and water absorption is obtained, and a simple calculation method for shale stress around the wellbore under hydration swelling is proposed ([11]). There is a chemical potential difference between the drilling fluid and the low-permeability shale formation fluid [12], and the membrane efficiency of the drilling fluid and the formation fluid is obtained through experimental methods [5]; (4) based on the free energy of water molecules, the thermal-hydro-mechanical-chemical (T-H-M-C) coupled

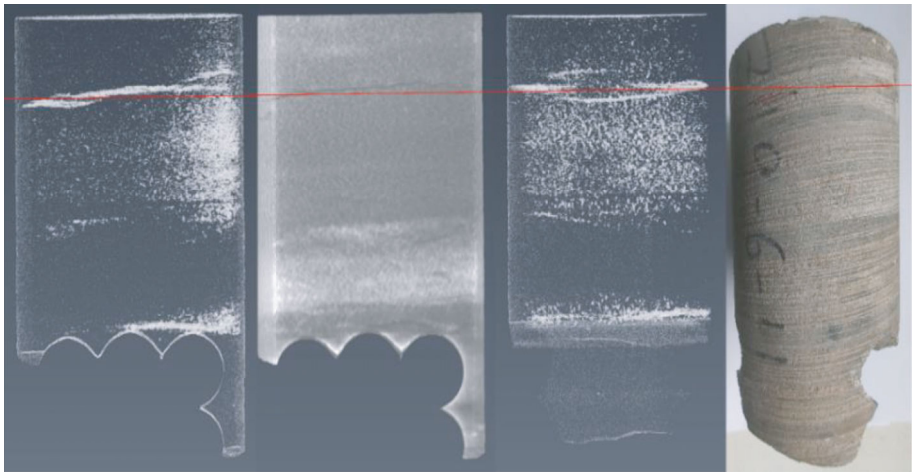

Figure 2: CT analysis of the middle-deep transition shale sample.

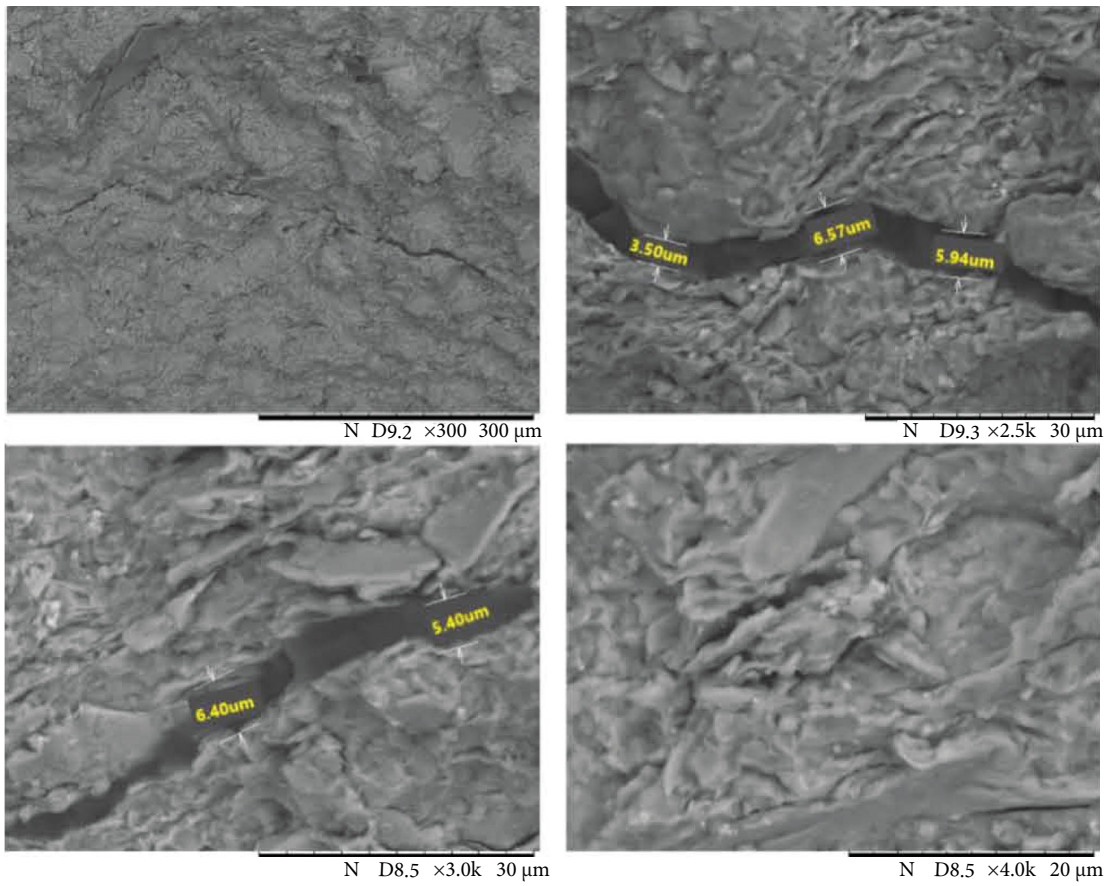

Figure 3: SEM analysis of internal structure of the middle-deep transition shale sample.

equations are derived [6]. Using the mechanical-chemical coupling model of porous media, the analytical expressions of ion concentration, pore pressure, and displacement are obtained. Thereby, the stress distribution around the wellbore can be obtained to analyze the influence of chemical and temperature factors on the stability of the chemically active shale formation [5]. The driving force of the interaction between drilling fluid and shale formation includes chemical potential difference and hydraulic pressure difference. It is believed that the membrane efficiency of low-permeability shale is about 1%~10% [13].

For brittle shale, the influence of shale-drilling fluid interaction on the strength of deep shale is analyzed through experiments [14]. The composition and structure of shale

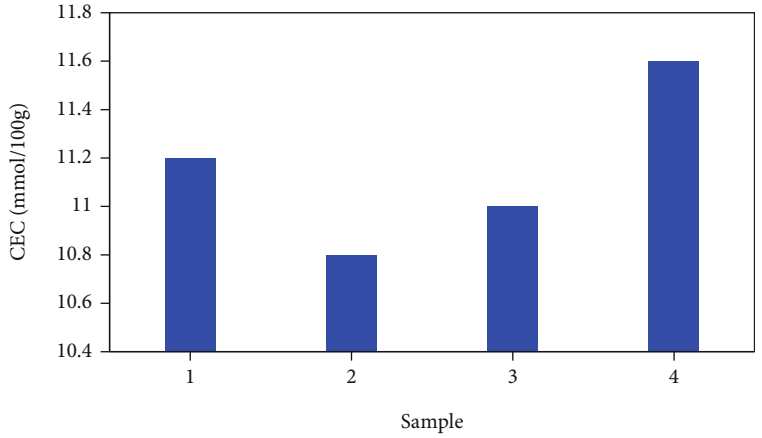

Figure 4: CEC values of the transition shale samples.

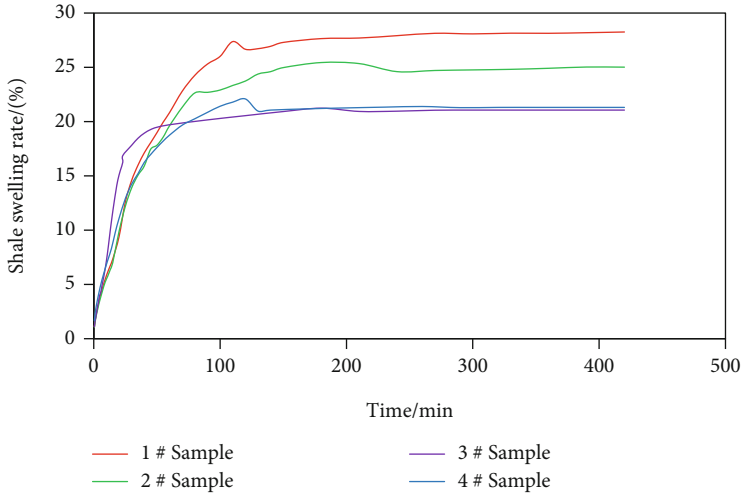

Figure 5: Swelling variation of the transition shale samples.

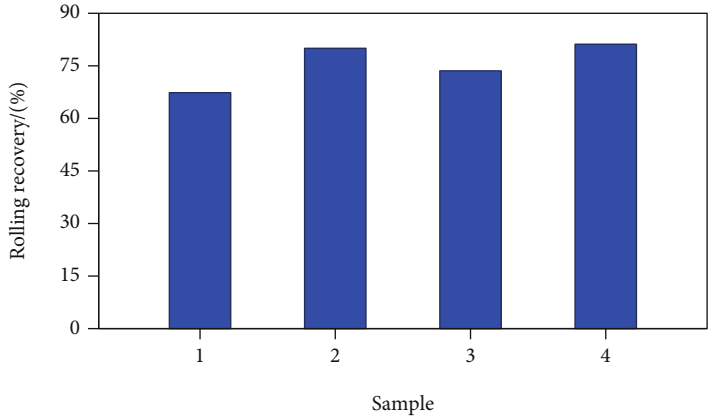

Figure 6: Shale dispersion in water testing results.

have an important influence on shale hydration swelling, and hydration swelling is the result of the coupling of physical and mechanical actions [15]. In addition, brittle shale has abundant bedding planes. The results show that the mechanical properties of samples with different angles of bedding plane are quite different [16]. Based on the linear

Figure 7: Debris from the middle-deep transition shale interval of Bohai oil field of China.

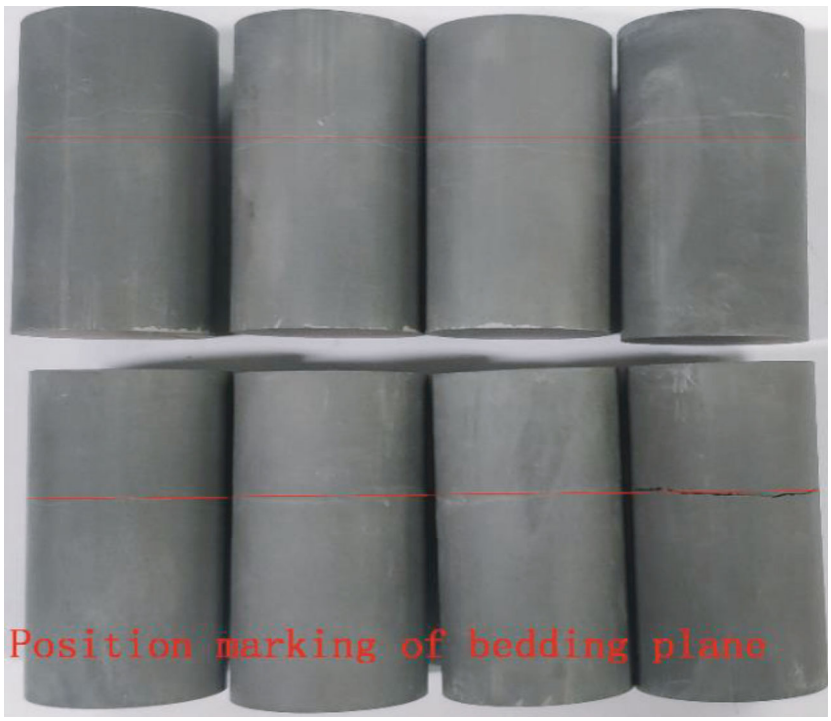

Figure 8: Transition shale samples for mechanical testing.

elastic wellbore stability mechanics model and single weak plane strength theory [17], a wellbore stability analysis model considering the influence of factors such as bedding plane strength, rock strength, horizontal well orientation, water content, and other factors has been established [18]. Further, there is a high contrast between the diffusion rate in the cracks and the porous matrix. The latter is regarded as an unsaturated stage and therefore does not participate in fluid transport. The effect of crack network length and rock properties on wellbore instability is analyzed [19]. Experiments show that the friction coefficient of the bedding plane can reduced by the penetration of drilling fluid filtrate,

Table 3: Rock mechanical testing results.

Sample	Confining pressure (MPa)	E (GPa)	Poisson's ratio	Compressive strength (MPa)
1	0	14.37	0.129	48.97
2	10	20.36	0.29	91
3	10	21.46	0.2	117
4	20	18.12	0.15	141.4

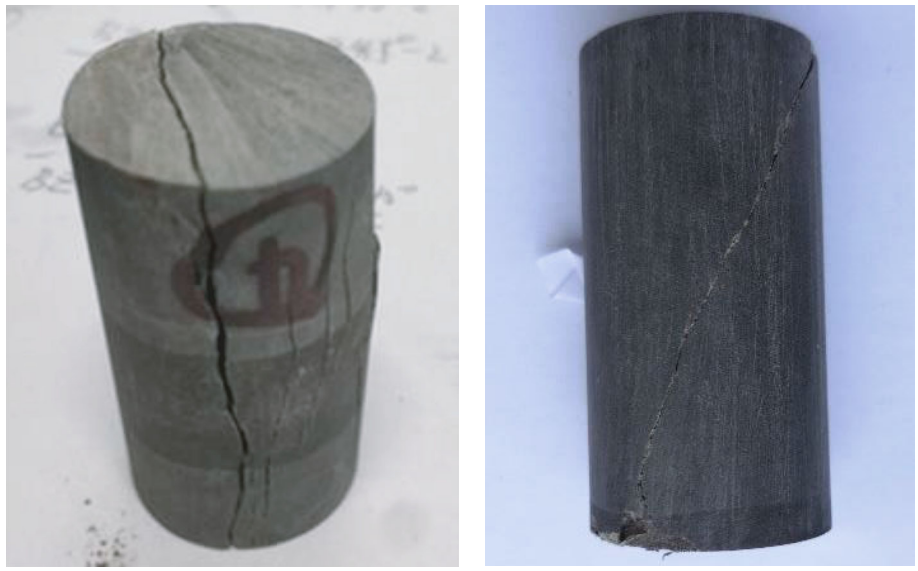

(a) (b)

Figure 9: Typical failure modes of shale samples in mechanical experiments.

Table 4: Direct shear testing results.

Sample	Shear area (mm^2)	Normal force (KN)	Normal stress (MPa)	Shear forces (KN)	Shear stress (MPa)
1	486.17	7.2	15	8.26	17
2	479.16	14.5	30	14.07	29.37
3	478.39	21.9	45	18.29	38.25

and the friction coefficient is more sensitive to oil-based drilling fluid filtrate than water-based [20].

Previous studies mainly focused on the stability of chemically active shale formation and the experimental study of shale-drilling fluid interactions leading to changes in strength. However, there are few studies on the mechanism of brittle shale wellbore instability. In this paper, laboratory experimental research and numerical simulation combined method reveals the mechanism of the instability of the middle-deep shale formation.

2. The Physical and Chemical Properties of Shale

The transition shale samples used in the experiment were taken from the middle-deep formation in Bohai oil field of China, and the depth of the formation is about 3600 meters. As shown in Figure 1, the size of shale sample is 100 mm in diameter and 180 mm in length.

Table 5: Strength parameters of the middle-deep transition shale samples.

Sample	C (MPa)	ϕ (°)
Rock matrix	8	35
Bedding plane	6.9	33

2.1. Composition and Structure of the Transition Shale. The X-ray diffraction (XRD) experiment was used to analyze the mineral composition and the clay mineral content of the transition shale. The results are shown in Tables 1 and 2. It can be seen that the mineral components of the

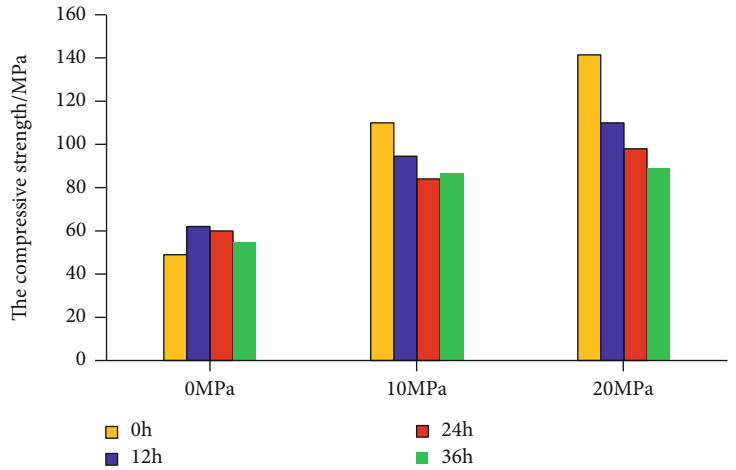

Figure 10: Strength of the middle-deep transition shale matrix after drilling fluid soaking.

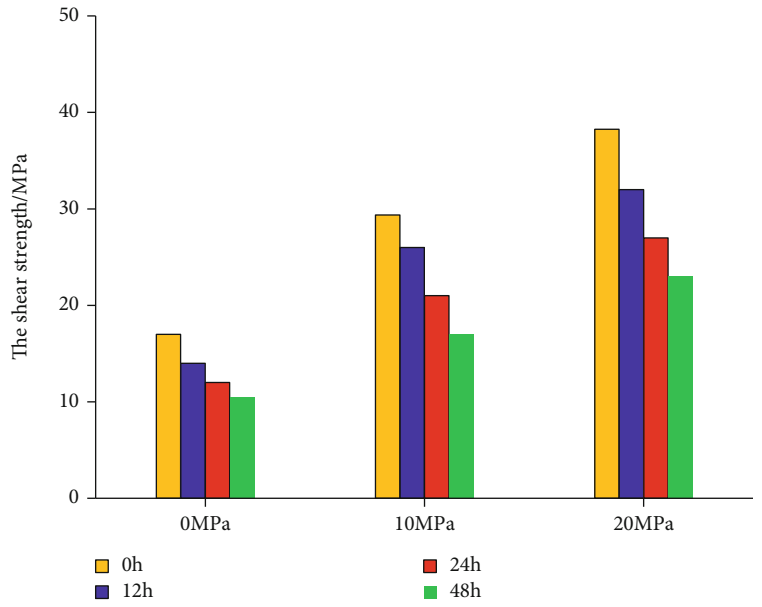

Figure 11: Strength of the bedding planes in the middle-deep transition shale after drilling fluid soaking.

transition shale are mainly clay and quartz. In addition, plagioclase, calcite, and dolomite are also present. Clay mineral amount ranges between 21.8% and 49.6%, with an average of 39.4%. Clay minerals are mainly mixed-layer illite-smectite (I/S) and illite (I), without pure montmorillonite (S), showing a certain swelling capacity. The quartz content ranges between 22.8% and 44.9%, with an average of 35%.

The microscopic structural characteristics of the middle-deep transition shale significantly affect its macroscopic mechanical properties. In order to study the microstructural characteristics of the middle-deep transition shale, the pore structure and microcracks were observed by computed tomography (CT) and scanning electron microscopy (SEM). As can be seen from Figures 2 and 3, the middle-deep transition shale formation develops near horizontal bedding planes and microcracks, of which the width ranges from 3.5 μm to 6.5 μm.

2.2. Analysis of Physical and Chemical Characteristics. The cation exchange capacity (CEC) tests [21] of four middle-deep transition samples were conducted. As can be seen from Figure 4, CEC values average 11.2 mmol/100 g and range between 10.8 mmol/100 g and 11.6 mmol/100 g. According to Figure 5, the swelling rate of the middle-deep transition shale in water increases rapidly with time in the early stage but reaches stability after a certain time, and the final swelling rate of the shale ranges from 21% to 28%. The rolling recovery experiment in water was conducted using rock debris at 130°C. The experimental results are shown in Figure 6, indicating that the rolling recovery [22] of shale ranges from 67% to 81%.

Based on the above laboratory experimental results of shale composition, structural, physical, and chemical characteristics, it is noted that content of brittle mineral and clay mineral is very high in the component, showing moderate

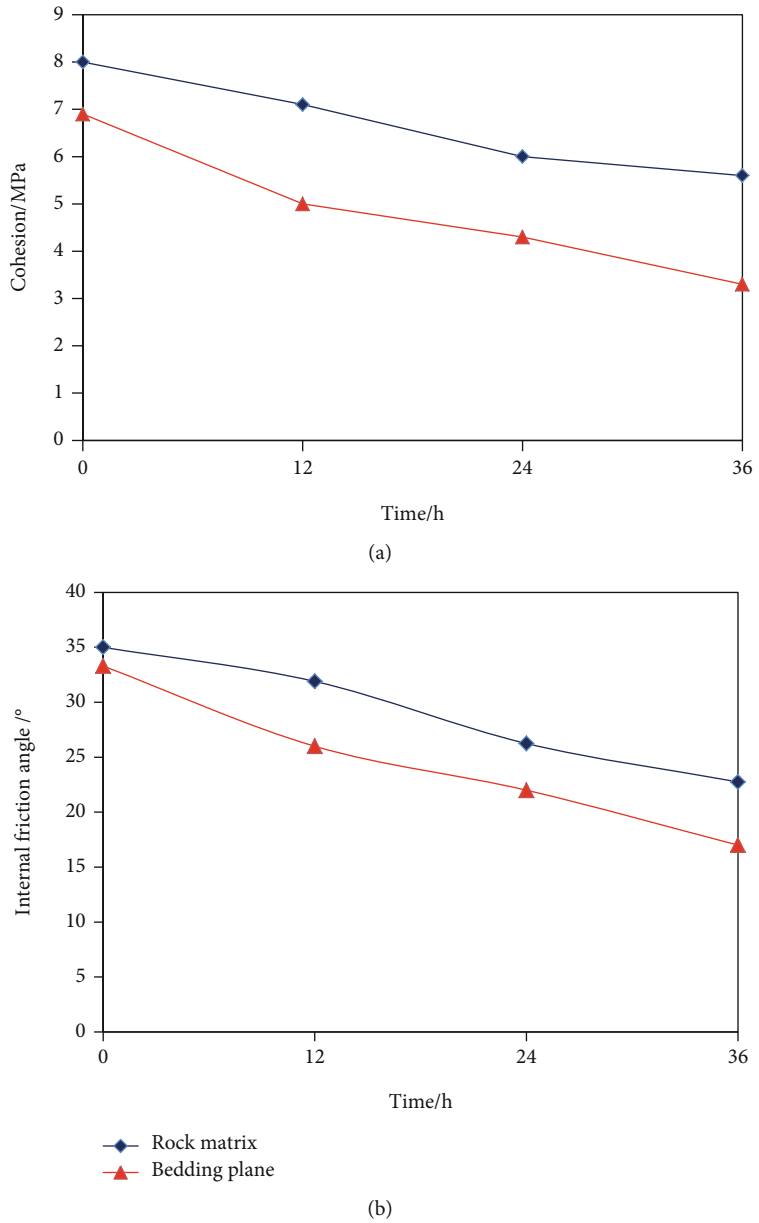

Figure 12: Curve of strength parameter of shale bedding plane and matrix in different soaking time.

swelling and dispersion, and has a certain hydration effect. In addition, microcracks and bedding planes are rich in the middle-deep transition shale formation. The experimental results show that the middle-deep shale in the Bohai oil field belongs to transition shale formation from shallow soft shale to deep brittle shale [23]. This type of shale features both structural weak planes and hydration swelling.

3. Mechanical Properties of Shale

The rock debris gathered from the drilling process is shown in Figure 7, and most of them are plate-like, indicating that there are abundant bedding planes and microcracks in the transition shale formation. The mechanical properties of rock are the key to study the wellbore stability of formation. Bedding plane has important impact on strength of the transition shale formation. In order to analyze the mechanical properties of this type of transition shale, we assume that the transition shale is composed by 2 parts, shale matrix and bedding planes. In order to fully understand the strength characteristics of the transition shale matrix and bedding planes, shale samples were drilled from preserved cores in the form of 25 mm diameter and 50 mm length cylinders taken parallel to the natural bedding planes. CT scanning experiment can accurately locate the position of the bedding plane. Figure 8(b) marks the position of the bedding plane of the standard shale sample. We use two methods to obtain the strength of shale matrix and bedding plane, respectively.

Table 6: Parameters used in the wellbore stability analysis considering the pore pressure and stress change due to the chemical effect.

Parameters	Values
Wellbore radius, r_w (m)	0.1
Young's modulus, E (GPa)	15.0
Poisson's ratio, ν	0.189
Undrained Poisson's ratio, ν_u	0.31
Pore pressure, p_0 (MPa)	48.60
Maximum horizontal stress, σ_H (MPa)	73.80
Minimum horizontal stress, σ_h (MPa)	64.80
Vertical stress, σ_V (MPa)	81.36
Mud pressure, p_m (MPa)	52.20
Pore solute concentration, C_0^S	0.20
Mud solute concentration, C_m^S	0.1
Swelling coefficient, ω_0 (MPa)	2.0
Permeability coefficient, κ (m^2(PA·s))	$1.28 * 10^{-17}$
Strata temperature, T (°C)	12
Porosity, ϕ	0.1
Reflection coefficient, $\mathfrak{R}$	0.2
Molar mass of solute (NaCl), M^S (g/Mol)	58.5
Fluid bulk modulus, K_f (GPa)	2.20
Solid bulk modulus, K_S (GPa)	48.2
Solute diffusion coefficient, D^S(m^2/s)	$5.0 * 10 - 9$
Rock matrix cohesion, C (MPa)	8
Internal friction angle of rock matrix, φ (°)	35

On the one hand, the strength parameters of shale matrix were measured by uniaxial and triaxial tests using standard samples obtained perpendicular to the bedding plane. The bedding planes and microcracks near the horizontal direction do not affect the strength of shale matrix. The experimental results are shown in Table 3. It can be seen from the table that the strength of the shale matrix is high.

By observing the failure mode of the shale, we can see that under uniaxial conditions, the failure mode of rock is splitting failure (Figure 9(a)). In the conventional triaxial compression test with confining pressure, the failure mode of the shale is shear failure (Figure 9(b)).

On the other hand, the YSZJ-30-50 multifunction direct shear apparatus was used to conduct direct shear experiment along the marked natural bedding planes, and the shear strength of bedding plane was directly measured. The shear tests were conducted at a normal stress range of 15~45 MPa. The experimental results are shown in Table 4.

From the results of uniaxial and triaxial experiments, the failure mode of the deep-middle transition shale matrix presents obvious shear failure. The Mohr-Coulomb criterion is used to describe the failure characteristics of the shale matrix, which can be expressed as follows:

$$\sigma_1 - \sigma_3 = \cot^2\left(45^\circ - \frac{\phi}{2}\right) + 2C\cot\left(45^\circ - \frac{\phi}{2}\right), \quad (1)$$

where C is the cohesion of rock matrix and ϕ is the internal friction angle.

The principle of direct shear experiment for shear strength is Coulomb criterion. The criterion holds that the shear strength is approximately linear with the normal stress when the normal stress is small. The formula is expressed as follows:

$$\tau = \sigma_n \tan\phi_w + C_w, \quad (2)$$

where C_w and ϕ_w are cohesion and internal friction angle of shear failure plane, respectively.

The shear strength parameters of the shale matrix and the bedding plane were obtained by linear fitting, and the results are shown in Table 5. It can be seen from Table 5 that the cohesion and internal friction angle of the shale matrix are larger than those of bedding plane. The results show that the bedding plane is a weak structural plane in the formation, and its cementation strength is weak. When the wellbore collapses, the bedding plane is often destroyed before the shale matrix.

Existing experimental results show that transition shale has hydration swelling properties. Drilling fluid diffuses into shale formation or invades into the formation along bedding plane or microcracks. In order to investigate chemical effects on the strength of the transition shale, the shale samples were soaked in the drilling mud for varying periods of time, and the uniaxial and triaxial compression experiments and direct shear experiments were conducted, respectively, to obtain the matrix strength and shear strength of the bedding plane. Considering the pressure difference between drilling mud and the formation pressure during the actual drilling process, the shale sample soaking pressure difference is set to be 3 MPa. And the drilling mud used in the experiment is the one used in the field. The experimental results of matrix strength after soaking for different time periods are shown in Figure 10, and those for the bedding plane are shown in Figure 11.

Compared with the results without soaking, the experimental results show that the shear strength of rock matrix and bedding plane decreases after soaking in drilling fluid, and the decrease trend of shear strength of bedding plane is more significant, indicating that the influence of drilling fluid immersion on the bedding plane is more significant.

Based on the Mohr-Coulomb criterion, the obtained experimental data were linearly fitted, and the internal friction angle and cohesion of bedding plane of the transition shale under different experimental conditions were obtained by linear fitting calculation. The results are shown in Figure 12. The experimental results show that after drilling fluid soaking, the shear strength of the bedding plane decreases by about 50%, and the shear strength of the shale matrix decreases by about 35%. Compared with the shale matrix, the bedding plane of shale is more easily affected by hydration, and in this case, the rock sample is easy to slip

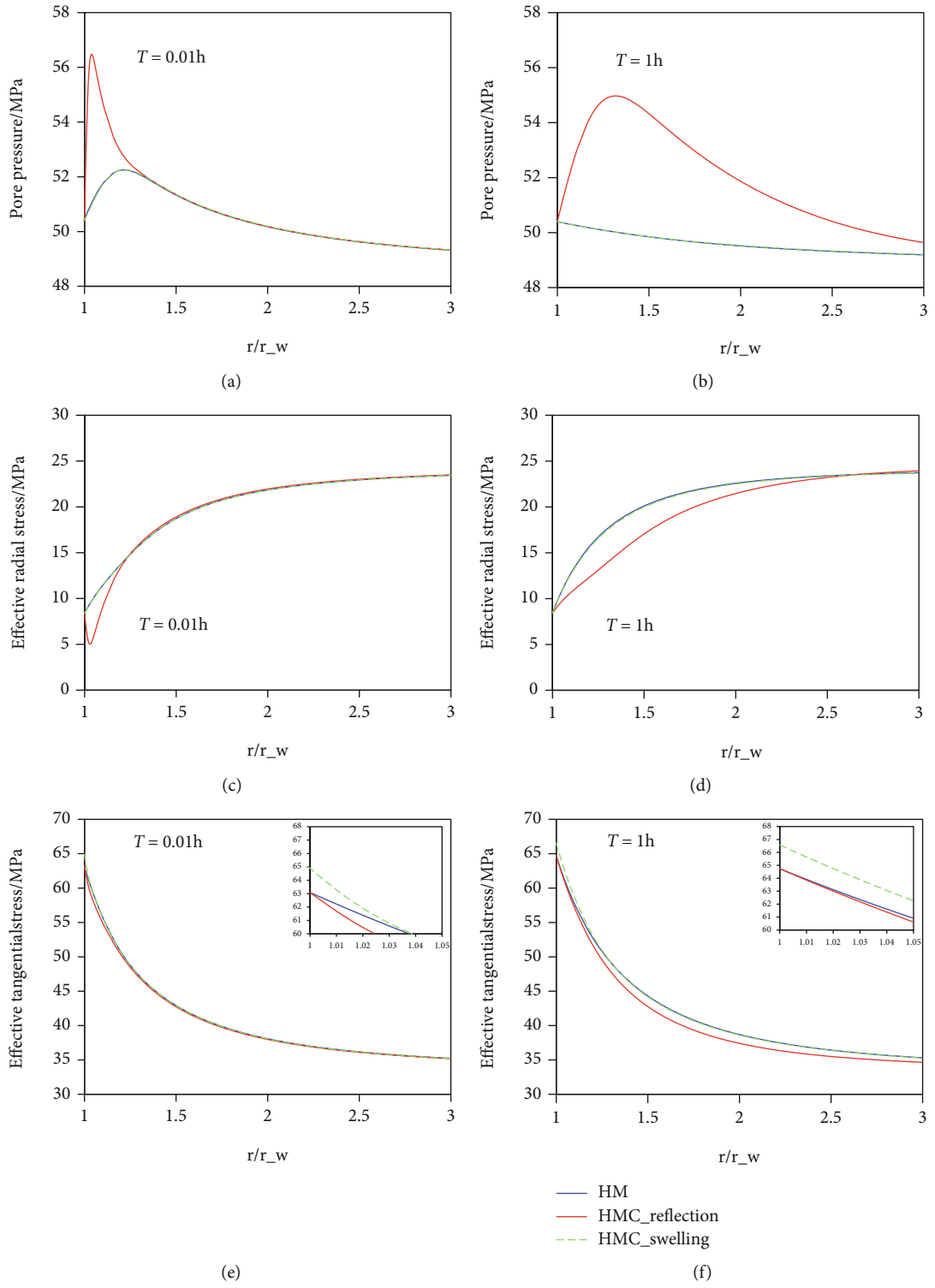

Figure 13: Pore pressure distribution around wellbore (a) 0.01 h and (b) 1 h after drilling; effective radial stress distribution around wellbore (c) 0.01 h and (d) 1 h after drilling; and effective tangential stress distribution around wellbore (e) 0.01 h and (f) 1 h after drilling.

along the bedding plane. The reason for that is that the bedding plane has relatively high permeability, compared to shale matrix. Therefore, it is easier for drilling fluid to penetrate into the bedding planes and reduce the strength.

On one hand, weak structural surfaces such as microcracks reduce the strength of the formation. On the other hand, it provides a channel for drilling fluid to invade the shale formation. After drilling the borehole, drilling fluid invades into shale along microcracks under hydraulic pressure difference and other driving forces. With the increase of pore pressure near wellbore, the interaction between drilling fluid and bedding plane clay minerals further

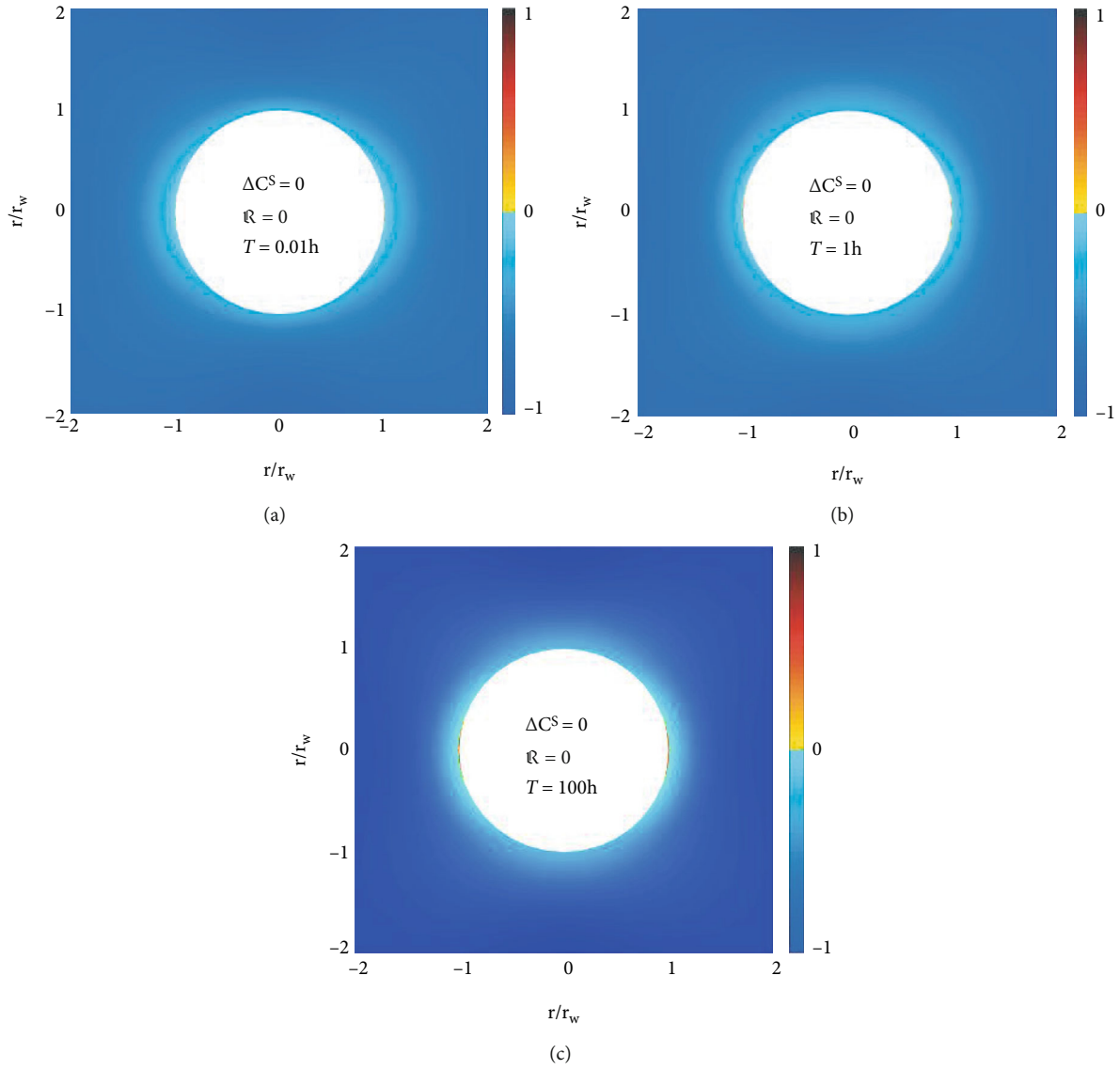

Figure 14: Damage zone around the wellbore considering hydromechanical coupling after (a) 0.01 h, (b) 1 h, and (b) 100 h drilling.

reduces the strength of bedding plane, resulting in the wellbore collapse of transition shale.

4. Analysis of Wellbore Instability Mechanism for the Transition Shale

Based on the composition and structural analysis and the experimental analysis results of physical and chemical properties, it can be seen that the middle-deep shale has brittle characteristics, moderate swelling and dispersion, and hydration swelling. In addition, the shale formation has rich bedding planes and microcracks. It means that the middle-deep shale belongs to the transition shale.

For this type shale, two major factors may simultaneously influence the wellbore stability. On the one hand, the chemical effect causes the change of pore pressure and swelling of the formation, which leads to the redistribution of effective stress around the wellbore. On the other hand, the formation is soaked in drilling fluid for a long time during the drilling process, which may result in penetration of drilling fluid along the bedding planes and the microcracks and thus reduction of the strength of the shale formation. In this paper, we analyze the two different mechanisms, respectively, and reveal the dominant mechanism of wellbore instability of the middle-deep transition shale.

4.1. Influence of Chemical Effects Induced Stress Redistribution on Wellbore Stability. Research of shale wellbore stability in recent years mainly focuses on the study of multifield coupling models such as mechanical-chemical coupling model. The mechanical-chemical coupling model mainly considers the chemical potential difference and hydraulic pressure difference to drive the mutual flow of drilling fluid and formation fluid, which leads to the change of pore pressure and effective stress around the wellbore and finally leads to the collapse around the wellbore.

The influence of chemical effect on pore pressure and effective stress around the wellbore can be simply divided

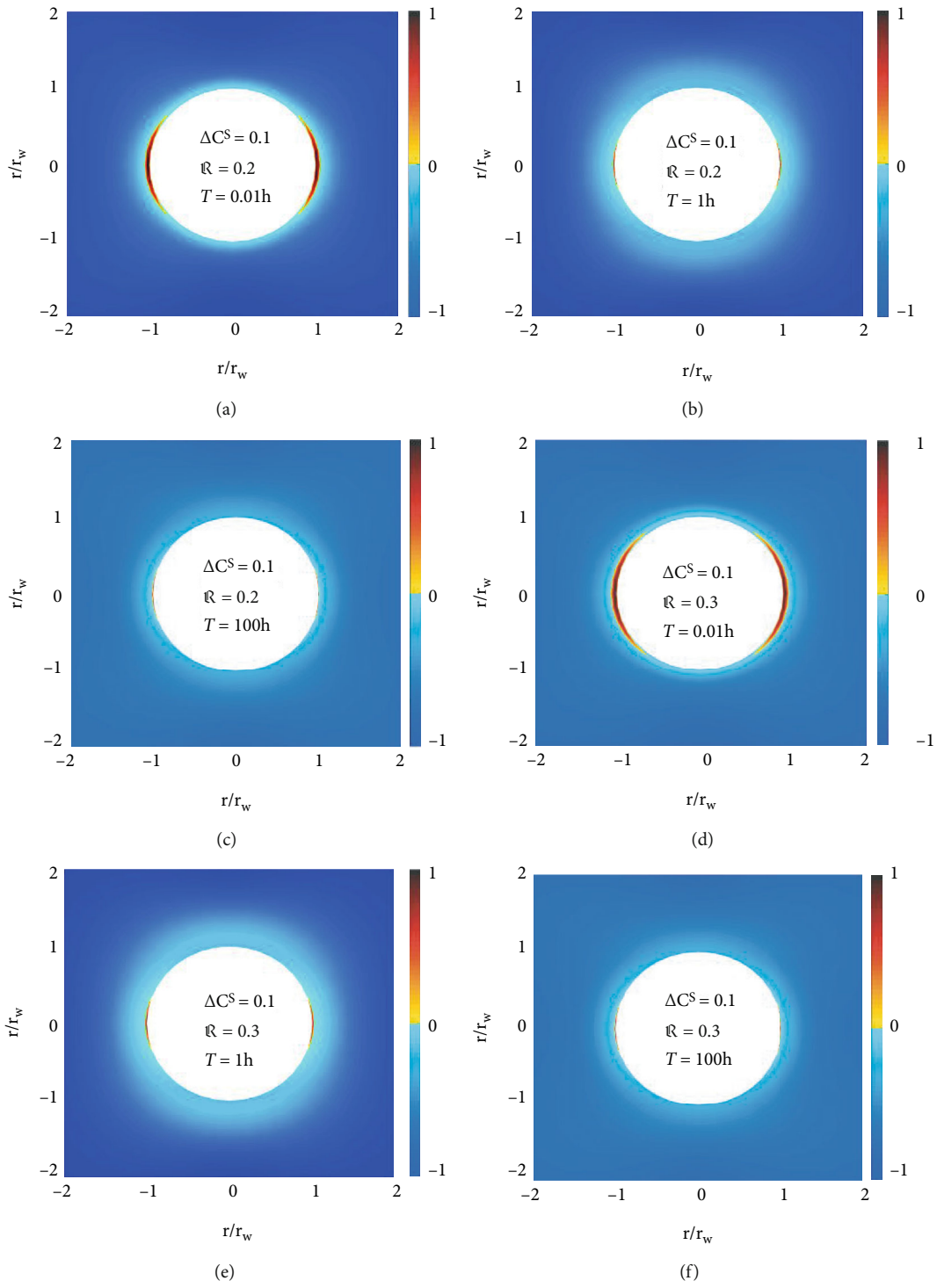

Figure 15: Continued.

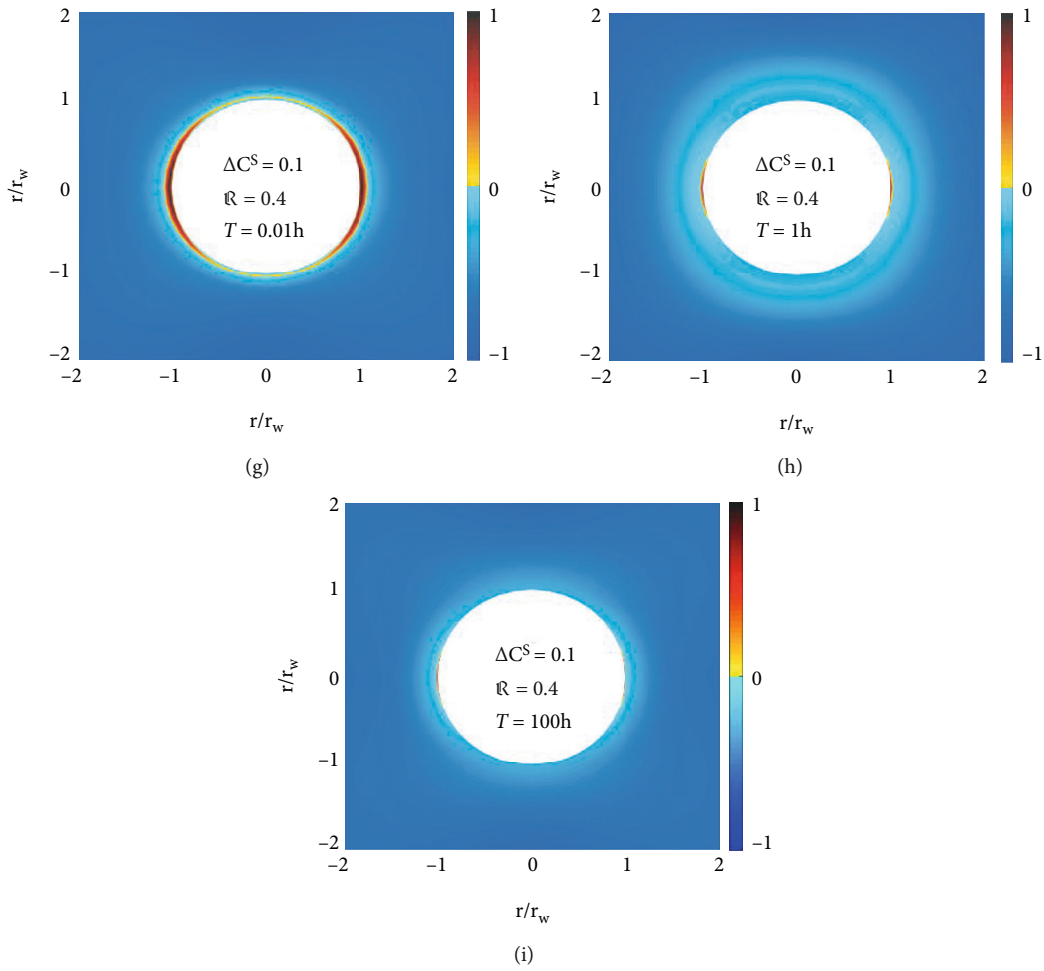

Figure 15: Damage zone around the wellbore (a) 0.01 h, (b) 1 h, and (c) 100 h after drilling for a reflection coefficient of 0.2; (d–f) for a reflection coefficient of 0.3; and (g–i) for a reflection coefficient of 0.4.

into two problems. One is that there is osmotic pressure between drilling fluid and formation fluid, and the drilling fluid diffuses into the formation through low-permeability mud shale, resulting in changes of pore pressure and effective radial stress around the wellbore. On the other hand, the mud shale formation is characterized by moderate swelling and dispersion. When drilling fluid flows into the formation and interacts with the clay minerals in the formation, the shale swells, and the effective tangential stress around the wellbore changes due to the far-field stress and compaction. The combination of these two problems results in a redistribution of effective stress and pore pressure around the wellbore after drilling.

Shale generally has the characteristics of low permeability. Diaz Perez [24] and Ghassemi et al. [6] suggested that there was a chemical potential difference and hydraulic pressure difference between the drilling fluid and the formation fluid in the low-permeability shale. When the formation solute concentration is larger than the drilling fluid solute concentration, the drilling fluid diffuses into the formation from the wellbore under the driving force of chemical difference in the wellbore, resulting in the increase of pore pressure. The hydration swelling between drilling fluid and clay mineral results in the change of stress. The procedure for solving the effective stress field around the wellbore considering the poro-chemo-mechanical coupling has been developed by Ghassemi and Diek [25] and Diaz Perez [24]. The problem is decoupled into three modes and solved separately and then superimposed together according to the methodology of Detournay and Cheng [26]. The detailed solutions of the stress distribution around the well affected by chemical factors are summarized below.

4.1.1. Mode I. The boundary condition of the first loading mode is that solute mass fraction and pore pressure are zero. So, the solution references the classical solutions in elasticity [26].

$$\sigma_{rr}^{(1)} = (P_0 - p_m)\frac{r_w^2}{r^2},$$
$$\sigma_{\theta\theta}^{(1)} = -(P_0 - p_m)\frac{r_w^2}{r^2}, \tag{3}$$

where r_w is borehole radius, r the radius around the well, and p_m the mud pressure. The mean stress P_0 and the deviatoric stress S_0 are expressed as

$$P_0 = \frac{\sigma_{xx} + \sigma_{yy}}{2} S_0 = \frac{\sqrt{\left(\sigma_{xx} + \sigma_{yy}\right) + 4\sigma_{xy}{}^2}}{2}. \quad (4)$$

4.1.2. Mode II. Mode II considers a virgin pore pressure and chemical loading at the wellbore wall. The solution of mode II is obtained by using the Laplace transform technique and then inverted to the time domain using the Stehfest algorithm. In the Laplace domain, the solution is

$$p^{(2)} = \left[(p_m - p_0) - \frac{\lambda_p^S (C_m^S - C_0^S)}{1 - \lambda_p^f/\lambda_C^S}\right] \frac{K_0(\xi_1 r)}{K_0(\xi_1 r_w)} + \frac{\lambda_p^S}{1 - \lambda_p^f/\lambda_C^S} \frac{(C_m^S - C_0^S)}{s} \frac{K_0(\lambda r)}{K_0(\lambda r_w)},$$

$$C^{(2)S} = \frac{C_m^s - C_0^s}{s} \frac{K_0(\lambda r)}{K_0(\lambda r_w)},$$

$$s\sigma_{rr}^{(2)} = \frac{(1-2\nu)\alpha}{(1-\nu)} \left\{ \begin{array}{l} \left[(p_m - p_0) - \dfrac{\lambda_p^S (C_m^S - C_0^S)}{1 - \lambda_p^f/\lambda_C^S}\right] \left[\begin{array}{l} \dfrac{K_1(\xi_1 r)}{r\xi_1 K_0(\xi_1 r_w)} \\ -\dfrac{r_w K_1(\xi_1 r_w)}{r^2 \xi_1 K_0(\xi_1 r_w)} \end{array} \right] \\ + \dfrac{\lambda_p^S (C_m^S - C_0^S)}{1 - \lambda_p^f/\lambda_C^S} \left[\dfrac{K_1(\lambda r)}{r\lambda K_0(\lambda r_w)} - \dfrac{r_w K_1(\lambda r_w)}{r^2 \lambda K_0(\lambda r_w)}\right] \end{array} \right\}$$
$$+ \frac{2G\beta(1+\nu)}{3(1-\nu)} \left(C_m^S - C_0^S\right) \left[\frac{K_1(\lambda r)}{r\lambda K_0(\lambda r_w)} - \frac{r_w K_1(\lambda r_w)}{r^2 \lambda K_0(\lambda r_w)}\right],$$

$$s\sigma_{\theta\theta}^{(2)} = -\frac{(1-2\nu)\alpha}{(1-\nu)} \left\{ \begin{array}{l} \left[(p_m - p_0) - \dfrac{\lambda_p^S (C_m^S - C_0^S)}{1 - \lambda_p^f/\lambda_C^S}\right] \left[\begin{array}{l} \dfrac{K_1(\xi_1 r)}{r\xi_1 K_0(\xi_1 r_w)} \\ -\dfrac{r_w K_1(\xi_1 r_w)}{r^2 \xi_1 K_0(\xi_1 r_w)} + \dfrac{K_0(\xi_1 r)}{K_0(\xi_1 r_w)} \end{array} \right] \\ + \dfrac{\lambda_p^S (C_m^S - C_0^S)}{1 - \lambda_p^f/\lambda_C^S} \left[\dfrac{K_1(\lambda r)}{r\lambda K_0(\lambda r_w)} - \dfrac{r_w K_1(\lambda r_w)}{r^2 \lambda K_0(\lambda r_w)} + \dfrac{K_0(\xi_1 r)}{K_0(\xi_1 r_w)}\right] \end{array} \right\}$$
$$+ \frac{2G\beta(1+\nu)}{3(1-\nu)} \left(C_m^S - C_0^S\right) \left[\frac{K_1(\lambda r)}{r\lambda K_0(\lambda r_w)} - \frac{r_w K_1(\lambda r_w)}{r^2 \lambda K_0(\lambda r_w)} + \frac{K_0(\xi_1 r)}{K_0(\xi_1 r_w)}\right], \quad (5)$$

where C_m^S is mud solute concentration; C_0^S is pore solute concentration; p_0 is pore pressure; α is the Biot coefficient; ν is Poisson's ratio; and G is the shear modulus.

$$a^D = \frac{1}{C^D} \quad a^S = \frac{1}{C^S} \quad \chi = \omega^0 \left(a^S - a^D\right) \quad B^D = -\frac{1}{3}\left(\frac{2\omega^D + \omega^{D'}}{K_S}\right),$$

$$B^S = -\frac{1}{3}\left(\frac{2\omega^S + \omega^{S'}}{K_S}\right) \Lambda = \left(Q + \frac{\phi}{K_f} + \frac{a^D B^D}{\rho_f}\right) a^D = \frac{1}{C^D} a^S = \frac{1}{C^S},$$

$$\tilde{\Omega} = \Omega + \frac{\breve{\rho}_{f0} RT}{M^S} \kappa \frac{\phi}{D^S} \mathfrak{R} a^S a^D \quad BB = \left(\alpha - \frac{c\omega^D}{\rho_f}\right) \quad \omega^S = \omega^D = \omega^0 \frac{Ms}{RT},$$

$$\lambda_p^S = \frac{\left(\alpha\chi - L_{11}\tilde{\Omega}\right)}{\Lambda L_{11} + \alpha BB} \quad \lambda_p^f = \frac{\kappa L_{11}}{\Lambda L_{11} + \alpha BB} \quad \lambda_{C^S}^S = \frac{D^S}{\phi}. \quad (6)$$

4.1.3. Mode III. The boundary condition of the third loading mode is to consider the wellbore stress solution under far-field eccentric loading. Then, the principal stresses in the plane can be written as

$$\frac{sp^{(3)}}{S_0 \cos 2\theta} = \frac{B^2(1-\nu)(1+\nu_u)^2}{9(1-\nu_u)(\nu_u - \nu)} C_1 K_2(\lambda r) + \frac{B(1+\nu_u) C_2}{3(1-\nu_u)} \frac{r_w{}^2}{r^2},$$

$$\frac{s\sigma_{rr}^{(3)}}{S_0 \cos 2\theta} = \frac{B(1+\nu_u)}{3(1-\nu_u)} C_1 \left[\frac{1}{(\lambda r)} K_1(\lambda r) + \frac{6}{(\lambda r)^2} K_2(\lambda r)\right] - \frac{C_2}{(1-\nu_u)} \frac{r_w{}^2}{r^2} - 3C_3 \frac{r_w{}^4}{r^4},$$

$$\frac{s\sigma_{\theta\theta}^{(3)}}{S_0 \cos 2\theta} = -\frac{B(1+\nu_u)}{3(1-\nu_u)} C_1 \left[\begin{array}{c} \dfrac{1}{(\lambda r)} K_1(\lambda r) \\ + \left(1 + \dfrac{6}{(\lambda r)^2} K_2(\lambda r)\right) \end{array} \right] + 3C_3 \frac{r_w{}^4}{r^4},$$

$$\frac{s\sigma_{r\theta}^{(3)}}{S_0 \sin 2\theta} = \frac{2B(1+\nu_u)}{3(1-\nu_u)} C_1 \left[\frac{1}{(\lambda r)} K_1(\lambda r) + \frac{3}{(\lambda r)^2} K_2(\lambda r)\right] - \frac{C_2}{2(1-\nu_u)} \frac{r_w{}^2}{r^2} - 3C_3 \frac{r_w{}^4}{r^4}, \quad (7)$$

where ν_u is undrained Poisson's ratio and θ is the angle between point on wellbore and maximum horizontal ground stress.

$$C_f = \frac{2kB^2 G(1-\nu)(1+\nu_u)^2}{9(1-\nu_u)(\nu_u - \nu)} \quad C_f = \frac{2kB^2 G(1-\nu)(1+\nu_u)^2}{9(1-\nu_u)(\nu_u - \nu)} \quad B = \frac{K_f}{\left(K_f + \phi K\right)},$$

$$K = \frac{E}{3(1-2\nu)} \quad D_1 = 2(\nu_u - \nu) K_1(\lambda r_w) \quad D_2 = \lambda r_w (1-\nu) K_2(\lambda r_w), \quad (8)$$

$$C_1 = -\frac{12\lambda w(1-\nu_u)(\nu_u - \nu)}{B(1+\nu_u)(D_2 - D_1)} \quad C_2 = \frac{4(1-\nu_u) D_2}{(D_2 - D_1)} \quad C_3 = -\frac{\lambda r_w (D_2 + D_1) + 8K_2(\lambda r_w)}{\lambda r_w (D_2 - D_1)}.$$

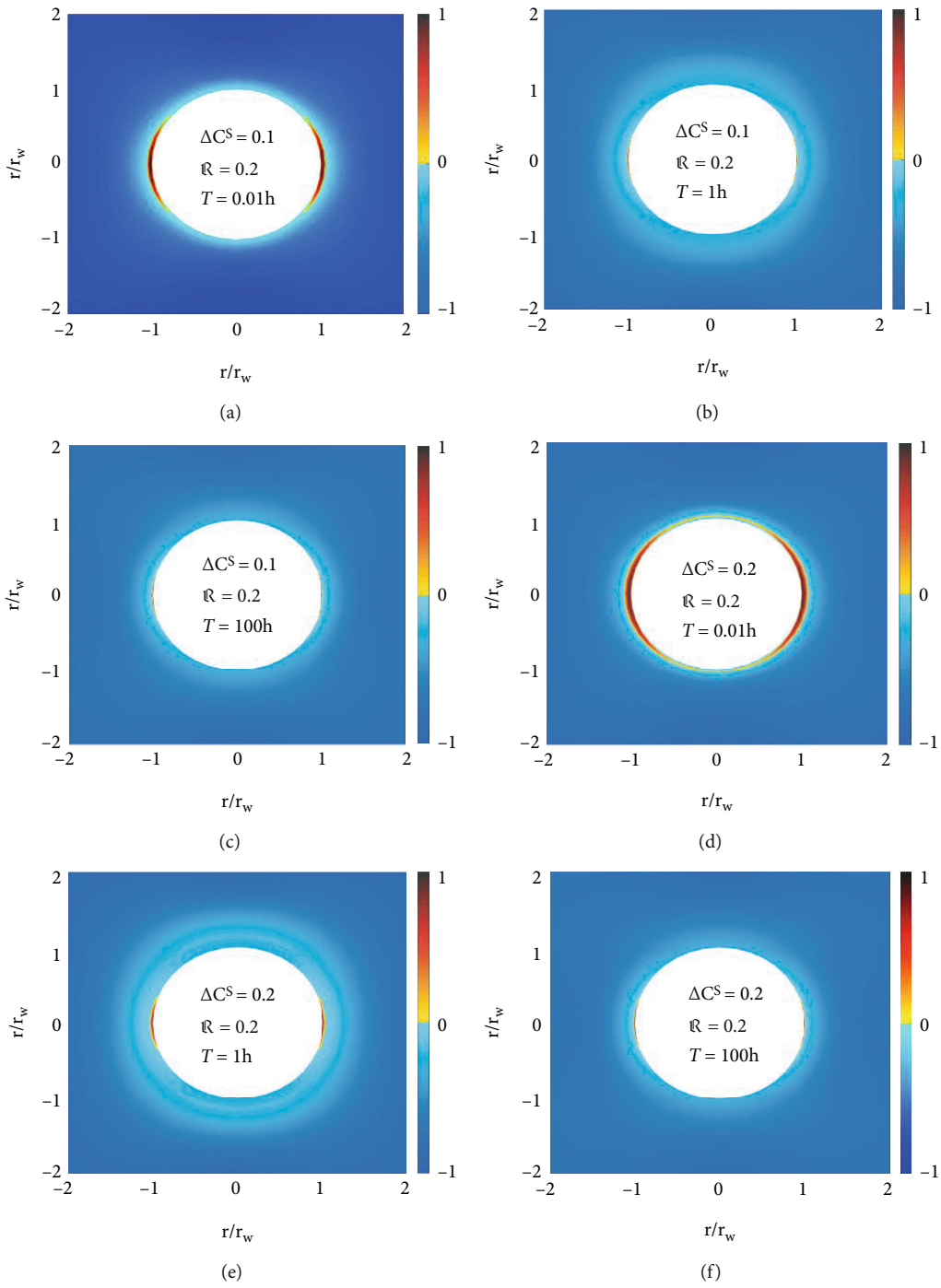

Figure 16: Continued.

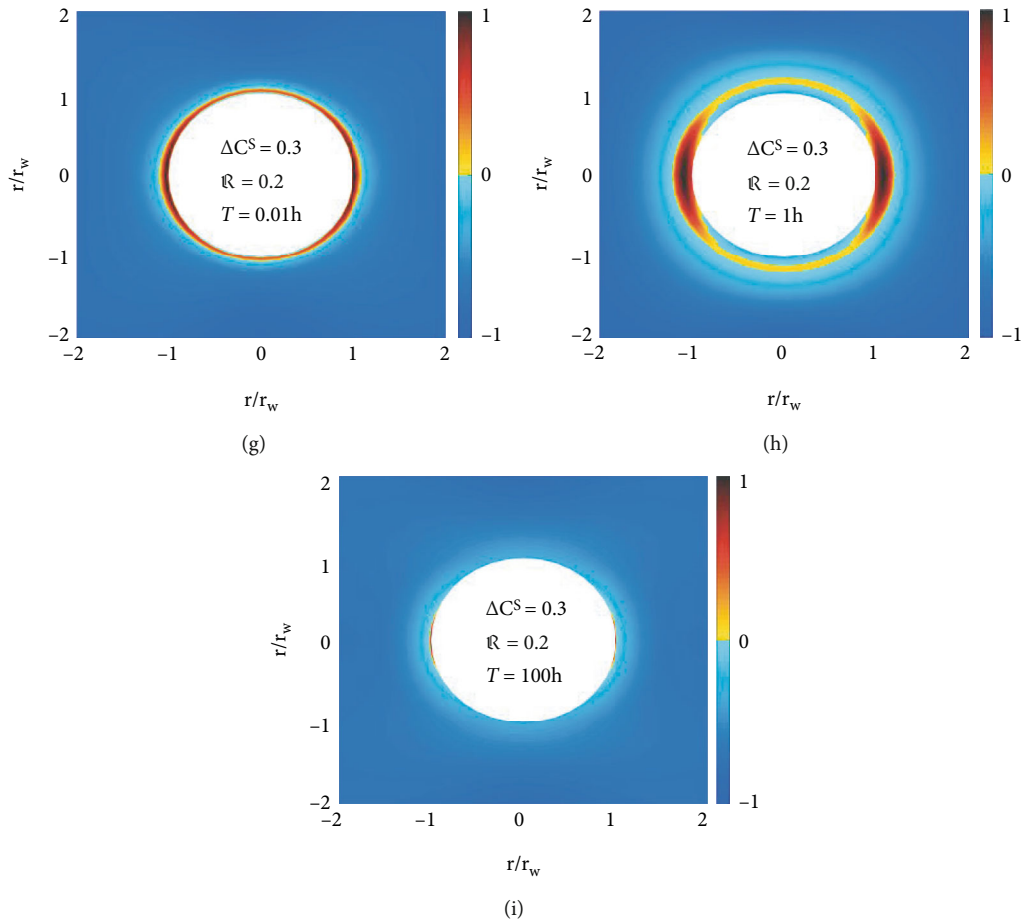

FIGURE 16: Damage zone around the wellbore (a) 0.01 h, (b) 1 h, and (c) 100 h after drilling for a solute concentration difference of 0.1; (d–f) for a solute concentration difference of 0.2; and (g–i) for a solute concentration difference of 0.3.

The final solution for the solute concentration, the pore pressure, and the stress distributions can be obtained by superimposing solutions from modes I to III onto the original stress, solute concentration, and pore pressure fields; i.e.,

$$\begin{aligned}
\sigma_{rr} &= -P_0 + S_0 \cos 2\theta + \sigma_{rr}^{(1)} + \sigma_{rr}^{(2)} + \sigma_{rr}^{(3)},\\
\sigma_{\theta\theta} &= -P_0 - S_0 \cos 2\theta + \sigma_{\theta\theta}^{(1)} + \sigma_{\theta\theta}^{(2)} + \sigma_{\theta\theta}^{(3)},\\
\sigma_{zz} &= -\sigma_z + \nu\left(\sigma_{\theta\theta}^{(1)} + \sigma_{\theta\theta}^{(2)} + \sigma_{\theta\theta}^{(3)}\sigma_{rr}^{(1)} + \sigma_{rr}^{(2)} + \sigma_{rr}^{(3)}\right)\\
&\quad - (\alpha - 2\nu\alpha)\left(p_0 + p^{(2)} + p^{(3)}\right) - \left(\chi' - 2\nu'\chi\right)C^S,\\
\sigma_{r\theta} &= -S_0 \sin 2\theta + \sigma_{r\theta}^{(3)},\\
p &= p_0 + p^{(2)} + p^{(3)},\\
C &= C_0^S + C^{(2)S}.
\end{aligned} \tag{9}$$

Based on the chemo-poro-elasticity theory established by Diaz Perez [24] and Ghassemi et al. [6], and combined with Mohr-Coulomb criterion in Equation (1), a coupling wellbore stability analysis model is established to discuss the influence of chemical effect on the wellbore stability of the transition shale.

Here, we consider a vertical well, named X1, in Bohai oil field of China. Severe well collapse happened when drilling to the shale interval located at the depth of 3877 m, and it was found that increasing the mud density merely could not solve the wellbore instability problem. The parameters used in the modeling are listed in Table 6.

Shale has very low permeability, and shale has the physical properties of semipermeable membrane, which can control the selective inflow and outflow of drilling fluid and formation water through semipermeable membrane. The reflection coefficient is used to characterize the membrane efficiency of the semipermeable membrane [27]. The reflection coefficient ranges from 0 to 1, and the closer the reflection coefficient to 1, the higher the membrane efficiency and the shale selectivity are. When the solute concentration in drilling fluid is greater than that in formation water, the free phase in formation water enters the wellbore through the shale semipermeable membrane under the action of chemical potential difference, resulting in the decrease of pore pressure and the change of stress around the wellbore. When the solute concentration in the drilling fluid is less than that

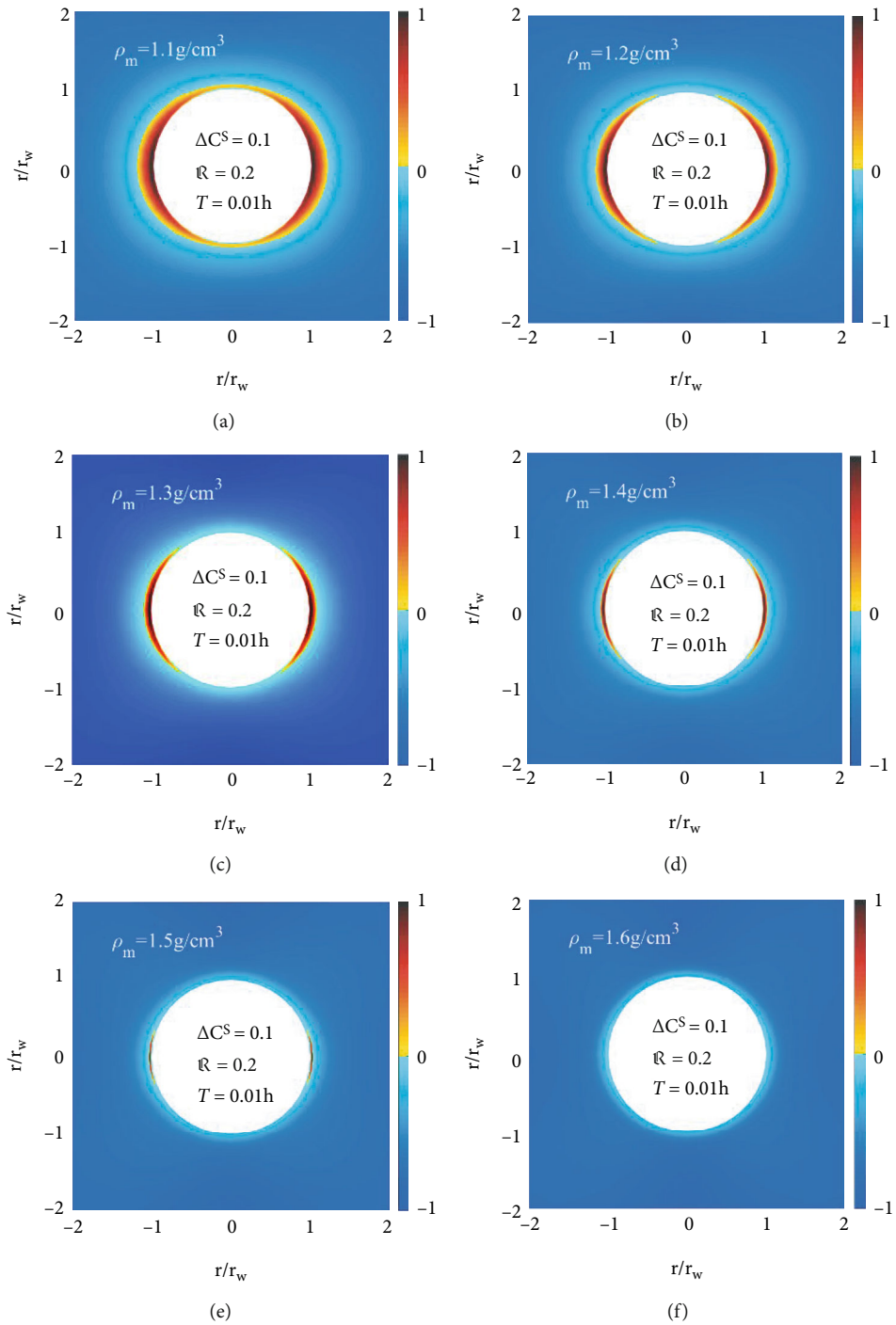

Figure 17: Damage zone around the wellbore for a mud density of (a) 1.1 g/cm^3, (b) 1.2 g/cm^3, (c) 1.3 g/cm^3, (d) 1.4 g/cm^3, (e) 1.5 g/cm^3, and (f) 1.6 g/cm^3.

in the formation water, the drilling fluid flows into the formation through the shale semipermeable membrane, resulting in the increase of the pore pressure around the wellbore and the change of the effective stress around wellbore. In addition, the drilling fluid flows into the formation and reacts with clay minerals in the formation, resulting in swelling pressure [28]. Through the above analysis, we take the situation that the solute concentration of drilling fluid is less than that of formation ($C_0^S > C_m^S$) as the analysis condition in this paper. The changes of pore pressure and effective stress around wellbore are caused by the diffusion of drilling fluid into the formation under the combined drive of chemical potential difference and hydraulic pressure difference. Firstly, the effects of swelling coefficient, reflection coefficient, and ion concentration difference on pore pressure and effective stress around wellbore are studied.

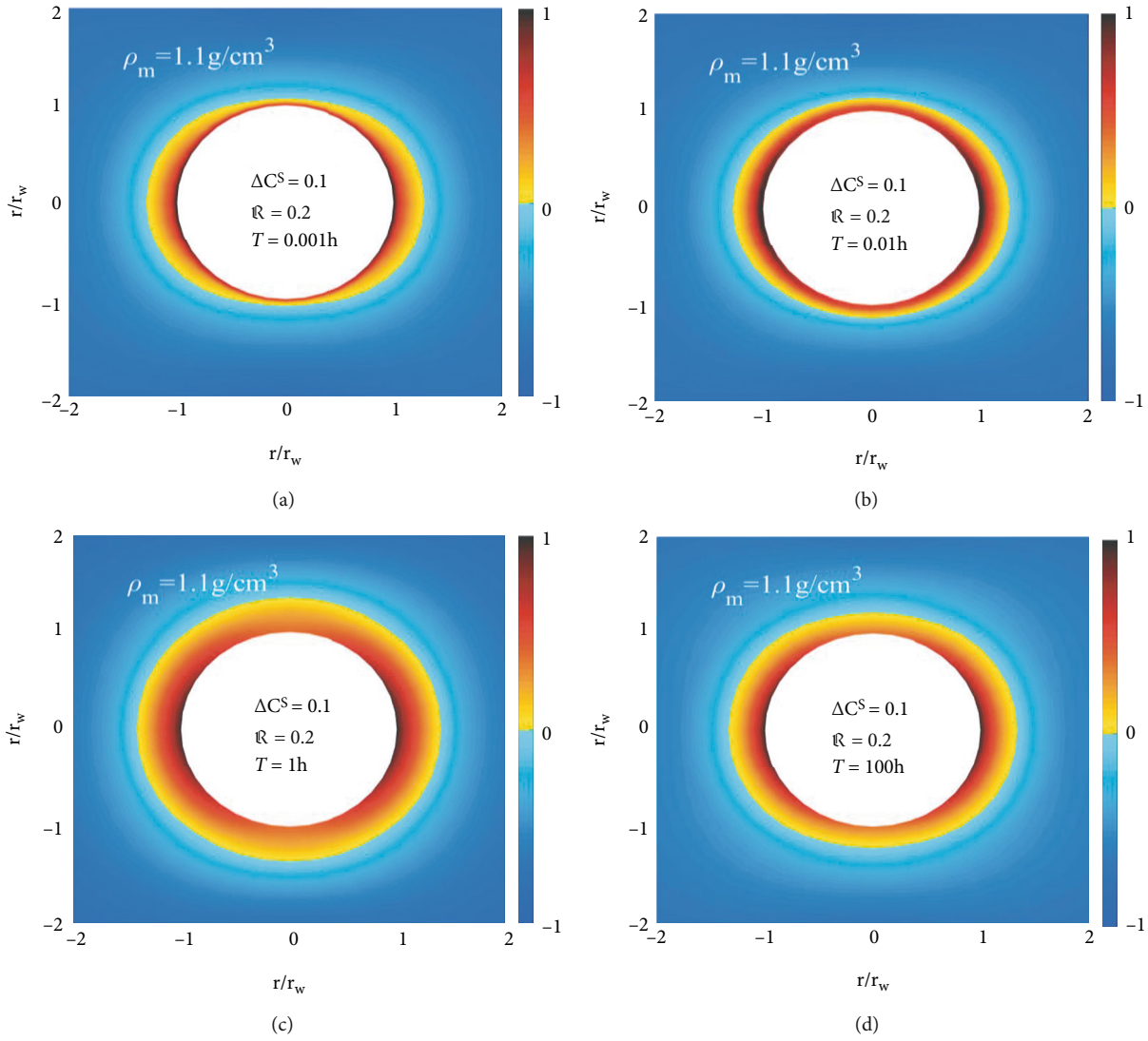

Figure 18: Damage zone around the wellbore of drilled in shallow soft shale (a) 0.001 h, (b) 0.01 h, (c) 1 h, and (d) 100 h after drilling.

Based on the above fully coupled H-M-C wellbore stability analysis model, we analyze the influence of partial H-M-C coupling model and fully coupled H-M-C model chemical factors on pore pressure and effective stress around the wellbore and compared with hydraulic-mechanical (H-M) coupling model, and we discuss the influence of reflection coefficient and swelling coefficient on stress distribution.

Figure 13 shows the distribution of pore pressure and effective stress around the wellbore for different models. Figure 13(a) shows the distribution of pore pressure around the wellbore of different models after 0.01 h of drilling. Compared with the H-M coupling model, it can be seen that the reflection coefficient leads to the increase of pore pressure, but the swelling coefficient has little effect on the pore pressure. Figure 13(b) shows the distribution of pore pressure after 1 h drilling. Compared with the distribution of pore pressure after 0.01 h drilling, it can be seen that with the increase of drilling time, the pore pressure diffuses and the maximum pore pressure around wellbore is reduced. Figure 13(c) shows the distribution of effective radial stress around wellbore for different models. Compared with the H-M coupling model, it can be seen that the reflection coefficient leads to the transformation of the effective radial stress around wellbore from compressive stress to tensile stress, but the swelling coefficient has little effect on the effective radial stress. Figure 13(d) shows the distribution of effective radial stress around wellbore after 1 h drilling. Compared with the distribution of effective radial stress after 0.01 h drilling, we can see that the effective radial stress changes along the wellbore diameter. Figures 13(e) and 13(f) show the distribution of effective tangential stress around wellbore for different models. Compared with H-M coupling model, we can see that reflection coefficient have little effect on effective tangential stress. However, when the hydration swelling effect of shale is taken into account. Higher tangential stress is induced due to chemical swelling of the formation. However, the tangential stress increase due to hydration swelling is not significant.

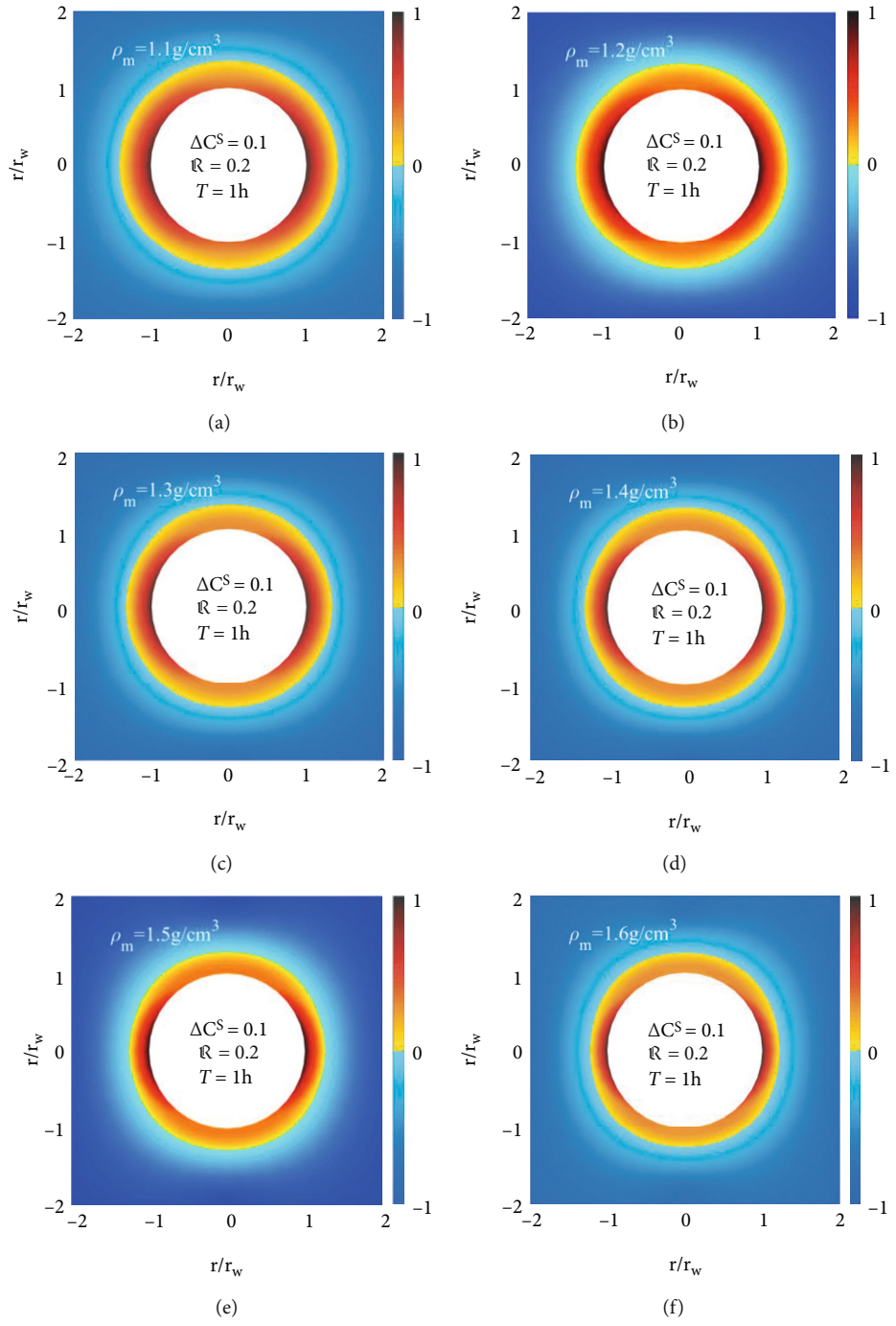

Figure 19: Damage zone around the wellbore of drilled in shallow soft shale for a mud density of (a) 1.1 g/cm^3, (b) 1.2 g/cm^3, (c) 1.3 g/cm^3, (d) 1.4 g/cm^3, (e) 1.5 g/cm^3, and (f) 1.6 g/cm^3.

Through the above analysis, we can see that the reflection coefficient and ion concentration have a great influence on the pore pressure and effective radial stress around wellbore, but the swelling coefficient has little effect on the stress around the well. So we analyze the influence of reflection coefficient and ion concentration difference on the wellbore stability of transition shale formation.

First of all, we separately discussed the size of the damage zone around wellbore for H-M coupling model after different drilling moments. In the figures, yellow and red represent the shear damage zone, and red represents the serious damage zone. Figure 14 shows the damage zone around wellbore after 0.01 h, 1 h, and100 h drilling, respectively. It can be seen that there is a very small damage zone in the minimum horizontal stress direction. And with the increase of time, the damage zone around wellbore shows an increasing trend. However, it cannot explain the phenomenon of large collapse of the transition shale formation.

Next, we discussed the influence of reflection coefficient on the wellbore stability of transition shale formation. Figure 15 shows the changes of damage zone around wellbore for different reflection coefficients. Figures 15(a)–15(g) show the size of wellbore damage zone for different reflection coefficients after 0.01 h. drilling. With the increase of reflection coefficient, the size of damage zone around wellbore gradually increases. It shows that the larger the reflection coefficient (membrane efficiency), the closer the shale as a semipermeable membrane to the ideal semipermeable membrane, and the more significant the effect of chemical effect on wellbore stability. With the increase of time, we can see that the size of the damage zone around wellbore decreases. It shows that the pore pressure diffuses faster along the hole diameter.

Finally, we discussed the influence of ion concentration difference on wellbore stability of transition shale formation. Figure 16 shows the changes of damage zone around wellbore for different ion concentration difference. Figures 16(a)–16(g) show the size of damage zone for different ion concentration difference after 0.01 h drilling. It can be seen that with the increase of the ion concentration difference between drilling fluid and formation water, the area of damage zone increases, especially when the ion concentration difference is 0.3. Figures 16(g)–16(i) show the size of the damage zone around the wellbore after drilling at different times. We can see that the size of damage zone increases first and then decreases. Compared with the reflection coefficient, we can see that the ion concentration difference has a greater impact on wellbore stability.

Compared with the H-M coupling model, the size of damage zone around the wellbore of the H-M-C coupling model increased. However, this degree of near-wellbore formation failure area is not enough to explain the large collapse block phenomenon in the drilling process.

The drilling fluid density is an important factor affecting wellbore stability. Figures 17(a)–17(f) show the damage zone around the wellbore for drilling fluid densities ranging from 1.1 g/cm^3 to 1.6 g/cm^3. Since there is a high-pressure zone in the transition shale formation in region X, a large damage zone will appear around the well when drilling under the condition of low-density drilling fluid, as shown in Figure 17(a). As we expected, with the increase of drilling fluid density, the damage zone of rock around wellbore decreased. When the drilling fluid density is 1.4 g/cm^3, there is a very small damage zone around the wellbore. When the drilling fluid density is up to 1.6 g/cm^3, there is no damage zone around the wellbore. According to the H-M-C coupling theory, the drilling safety can be guaranteed by only increasing the drilling fluid density during the drilling process of the transition shale. However, when the drilling fluid density is 1.4 g/cm^3 in the field drilling process, there is still a serious phenomenon of collapse around the wellbore. Obviously, the H-M-C coupling theory cannot explain this phenomenon.

In order to observe the influence of chemical factors on the wellbore stability of transition shale formation, H-M-C coupling wellbore stability model was used to discuss the wellbore stability of shallow soft shale. Compared with the transition shale, the strength of the shallow soft shale is low. The cohesion and internal friction angle of the shallow soft shale considered here are 2.5 MPa and 25°, respectively. And the equivalent density of pore pressure is 1.0 g/cm^3. The other parameters are shown in Table 6. Figure 18 shows the change of wellbore damage zone from 0.001 h to 100 h after drilling. Figure 18(a) shows that there is a large size of damage zone around the wellbore after the moment of drilling. Figure 18(b) shows the damage zone around the wellbore 0.01 h after drilling. Compared with the moment after drilling, the area of damage zone around the wellbore 1 h after drilling increases to about twice. Figures 18(c) and 18(d) show the damage zone around the wellbore 1 h after drilling and 100 h after drilling, respectively. The size of the damage zone decreases slightly, and the size of the damage zone around the wellbore tends to be stable, but there is still a large collapse area.

Table 7: Parameters used in the wellbore stability analysis considering the strength degradation due to the chemical effect.

Parameters	Values
Shale matrix cohesion, C (MPa)	8
Internal friction angle of shale matrix, φ (°)	35
Bedding plane cohesion, C_{W1} (MPa)	6
Internal friction angle of bedding plane, φ_{W1}(°)	26.25
Bedding plane cohesion, C_{W2} (MPa)	5.2
Internal friction angle of bedding plane, φ_{W2} (°)	22.75

Figure 19 shows the damage zone around the wellbore for drilling fluid densities of the shallow soft shale ranging from 1.1 g/cm^3 to 1.6 g/cm^3. When the drilling fluid density is 1.1 g/cm^3, there is a very large damage zone around the wellbore. We can find that with the increase of drilling fluid density, the damage zone around the wellbore gradually decreases. There is no high-pressure area in the shallow soft shale formation, but there is still a large damage zone around the well when the drilling fluid density increases to 1.6 g/cm^3. The calculation results show that the chemical factors of drilling fluid in soft shale formation are the main factors affecting wellbore stability. Simply increasing the density of drilling fluid cannot maintain wellbore stability. In this case, the plugging effect of drilling fluid should be improved.

Through the above calculation results, we can find that even considering the most critical parameters, X1 well will not experience an extensive zone of failure around the wellbore, indicating that the chemical effect, i.e., osmotic pressure and hydration swelling, is not the dominant mechanism responsible for the wellbore instability in the transition shale formation since its strength is relatively high. However, for shallow soft shale formation, the change of pore pressure and stress around the wellbore induced by the chemical effect indeed has a great influence on the wellbore stability.

4.2. Influence of Chemical Effects Induced Strength Degradation on Wellbore Stability. During the drilling process, the drilling fluid pressure replaces the original formation stress to support the wellbore. Due to the existence of

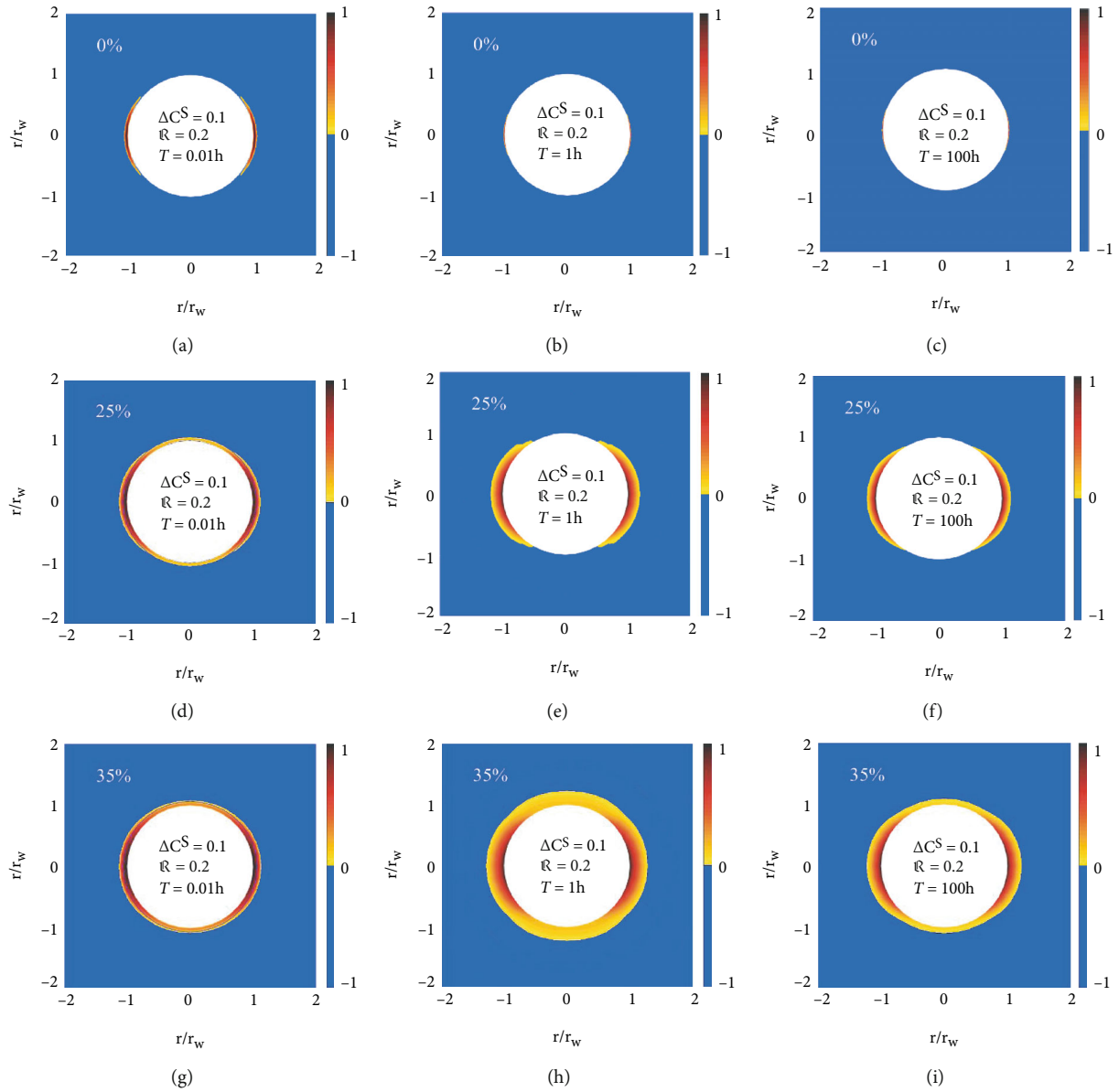

Figure 20: Damage zone around the wellbore (a) 0.01 h, (b) 1 h, and (c) 100 h after drilling for strength degradation of 0%; (d–f) for strength degradation of 25%; and (g–i) strength degradation of 35%.

hydraulic pressure difference and chemical potential difference, the drilling fluid flows into the formation. The hydration effect between the drilling fluid and the shale leads to the weakening of rock strength around the wellbore. Based on the above H-M-C coupling theory, this paper considered the weakening of shale strength caused by immersion to establish a wellbore stability model, and the influence of rock matrix and bedding plane strength degradation on borehole stability is discussed, respectively.

The results of shale soaking experiment in this paper showed that the strength weakening of the shale gradually tends to be gentle after 36 h of soaking. The calculation parameters used in the model are shown in Table 7, and the other parameters are shown in Table 6.

Figure 20 shows the damage zone around the wellbore with different weakening degrees of shale strength. Firstly, considering the model with no weakening of the shale matrix strength, we can see that there is a small damage zone around the wellbore after drilling in Figures 20(a)–20(c). Figures 20(d)–20(f) show the damage zone around the well with shale strength weakened by 25%. Compared with the model without weakening, we can see that the damage zone around the wellbore increased, but the scope of damage zone is small, which cannot explain the collapse phenomenon in the drilling process of transition shale formation. With the weakening of shale strength, the area of the damage zone around the wellbore increases gradually. Figures 20(g)–20(i) show the damage zone around the wellbore with the strength of shale weakened by 35%. Especially after 1 h of drilling, there is a large area of damage zone around the wellbore, which can well explain the phenomenon of returning to collapse and falling during the drilling.

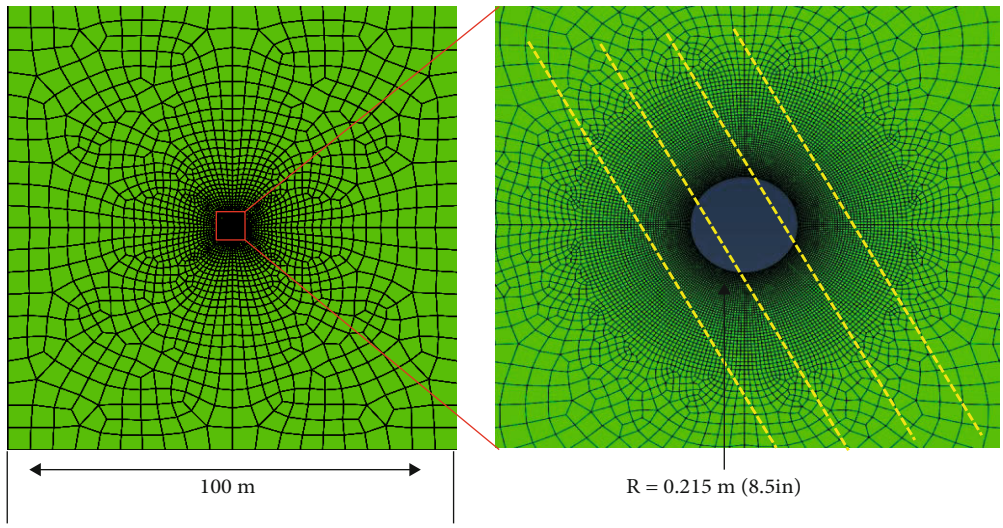

Figure 21: Geometry and mesh of the finite element model for the wellbore analysis considering fluid flow along the bedding planes as well as strength degradation of the bedding planes.

And the collapse area increases first and then decreases, indicating that 35% strength weakening has a serious impact on the wellbore stability.

There are abundant bedding planes and microcracks in the transition shale formation. The bedding strength is also an important factor for wellbore stability. In addition to the reduction of strength of shale matrix, the bedding strength is also greatly affected by drilling fluid immersion. Furthermore, the bedding planed and microcracks also provide pathways for drilling fluid to penetrate into the shale. Therefore, chemical reactions between drilling fluid and bedding plane clay minerals further reduce the strength of the bedding plane. It is more likely to lead to shear failure along the bedding planes and microcracks around the wellbore. To reveal the effect of strength degradation of the bedding planes and microcracks, we developed an elaborate finite element model as shown in Figure 21 using the well-known finite element package ABAQUS. The model employs a so-called jointed material model to characterize the effect of smeared parallel bedding planes and microcrack. In addition, the permeability of along the bedding planes and microcracks are set to be higher than that perpendicular the bedding planes and microcracks. The parameters used in the finite element modeling are listed in Table 8.

Based on the experimental results, the cohesion and internal friction angle obtained after soaking for different times were used for the bedding planes to analyze the influence of strength degradation of bedding planes and microcracks on the failure around the wellbore.

As a demonstration, considering a group of bedding planes and microcracks, the damage zone around the wellbore of the transition shale after drilling is shown in Figure 22. Figure 22(a) shows the shear damage zone of surrounding rock without considering bedding planes and microcracks. It can be seen that there is a small damage zone in the direction of minimum horizontal stress, which cannot explain the serious wellbore collapse observed in the field.

Table 8: Parameters used in the finite element modeling.

Parameters	Values
Wellbore radius, r_w (m)	0.1
Young's modulus, E (GPa)	15.0
Poisson's ratio, ν	0.189
Undrained Poisson's ratio, ν_u	0.31
Pore pressure, p_0 (MPa)	48.60
Maximum horizontal stress, σ_H (MPa)	73.80
Minimum horizontal stress, σ_h (MPa)	64.80
Vertical stress, σ_V (MPa)	81.36
Mud pressure, p_m (MPa)	52.20
Matrix permeability, K (mD)	0.02
Bedding permeability, K_W (mD)	0.2
Blocking efficiency	0.10
Rock matrix cohesion, C (MPa)	8
Internal friction angle of rock matrix, φ (°)	35
Bedding plane cohesion, C_W (MPa)	6
Internal friction angle of bedding plane, φ_W (°)	32

Figure 22(b) depicts the damage zone around the wellbore when bedding planes and microcracks are considered but without strength degradation and pore pressure change due to drilling fluid penetration, which shows a different pattern of damage; however, the damage zone size is still limited. When pore pressure increase due to drilling fluid penetration along the bedding planes and microcracks is taken into account, the size of the damage zone increases significantly as shown in Figure 22(c). Finally, if strength degradation and pore pressure increase are both considered, and the size of the damage zone is increased to about 3~4 times of the well diameter, which may result in severe wellbore collapse as observed in the actual drilling process of the X1 well considered in this paper.

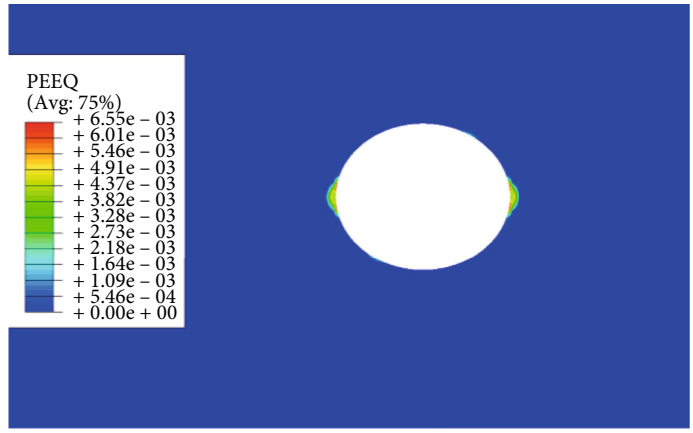

(a)

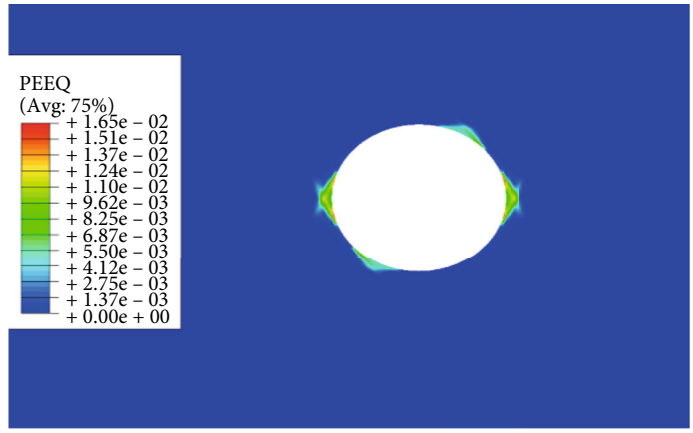

(b)

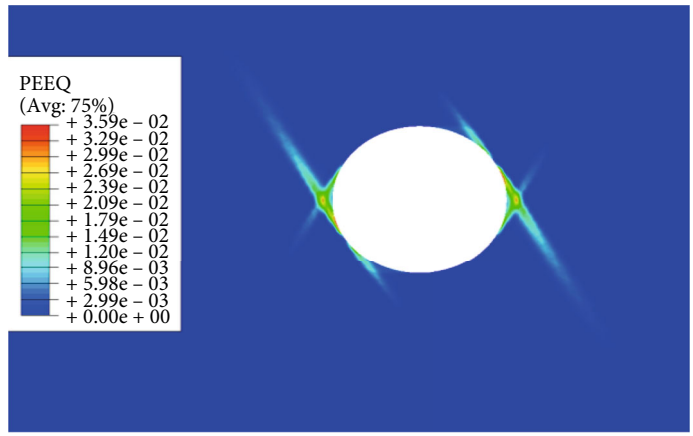

(c)

Figure 22: Continued.

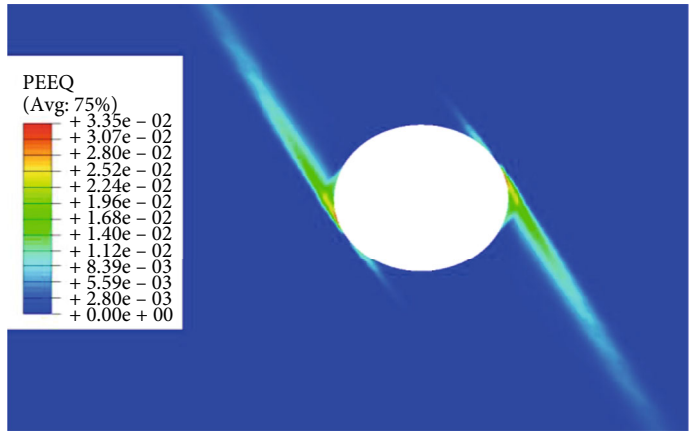

(d)

Figure 22: Damage zone around the wellbore (a) without considering the bedding planes and microcracks, (b) considering the bedding planes and microcracks without strength degradation and pore pressure change, (c) considering the bedding planes and microcracks with pore pressure change but no strength degradation, and (d) considering the bedding planes and microcracks with both strength degradation and pore pressure change.

4.3. Mechanism of Wellbore Instability in the Middle-Deep Transition Shale Formation. From the above analysis of the effects of redistribution of effective stress and the strength degradation caused by the chemical effect on the wellbore stability of the transition shale, it can be clearly observed that the extent of the damage zone around the wellbore is generally limited if only pore pressure change resulted from chemical potential difference and hydration swelling, which cannot explain the severe wellbore collapse observed the field drilling. In contrast, strength degradation due to the drilling fluid-shale interaction may greatly worsen the case, especially the strength degradation and pore pressure increase due to fluid penetration along the bedding planes and microcracks, which may generate a damage zone of 3~4 times of the well diameter, which fits the field observed phenomenon. Thus, the dominant mechanism responsible for the wellbore instability in the middle-deep transition shale can be attributed the bedding planes and microcracks, which provide pathways for drilling fluid penetration, resulting strength degradation and pore pressure increase. Thus, to maintain wellbore stability in this shale, it is the first priority to improve the sealing capability of the drilling fluid to prevent penetration of the drilling fluid into the bedding planes and microcracks.

5. Conclusions

In this paper, experimental testing and analytical and numerical analyses are performed to reveal the dominant mechanism of the wellbore instability in the middle-deep shale in the Bohai oil field of China. It is evidenced from the experiments that the middle-deep shale features both medium chemical activity and abundant bedding planes and microcracks. Thus, from the diagenesis perspective, the middle-deep shale is in the transition process from chemically actively soft shale to the chemically inactive but laminated and fractured hard shale. Mechanical testing shows considerable strength degradation of the middle-deep transition shale due to drilling fluid-shale interaction.

A hydro-chemo-mechanical coupling theory is first employed to characterize the effect of pore pressure change and hydration swelling caused by the chemical difference between drilling fluid and formation fluid on the stress distribution and thus the damage around the wellbore, which clearly demonstrates that the extent of the damage zone around the wellbore is limited if only pore pressure change and hydration swelling are considered which cannot explain the severe wellbore collapse in the drilling process. Furthermore, a finite element model is developed and used to demonstrate the effect of pore pressure increase and strength degradation of the shale due to drilling fluid penetration along the bedding planes and microcracks, which shows that a damage zone of 3~4 times of the well diameter can be generated, which may be the reason for the serious wellbore collapse experienced in the field.

From the experimental and analysis results, it is inferred that the dominant mechanism of the wellbore instability in the middle-deep transition shale formation in the Bohai oil field of China is the pore pressure change and strength degradation resulted from drilling fluid penetration along the bedding planes and microcracks. Thus, the best practice is to improve the plugging capability of the drilling fluid to reduce the penetration of drilling fluid into the bedding planes and microcracks, and tailoring the chemical activity of the drilling fluid to reduce the chemical potential difference between the drilling fluid and the formation fluid is not enough.

Data Availability

Data is available upon request.

Conflicts of Interest

The authors declare that they have no conflicts of interest.

References

[1] A. Ghassemi and A. Diek, "Linear chemo-poroelasticity for swelling shales: theory and application," *Journal of Petroleum Science and Engineering*, vol. 38, no. 3-4, pp. 199–212, 2003.

[2] A. Ghassemi, G. Wolfe, A. Diek, and J.-C. Roegiers, "A chemo-mechanical model for borehole stability analyses," in *Vail Rocks 1999, The 37th US Symposium on Rock Mechanics (USRMS)*, OnePetro, Colorado, 1999.

[3] F. Deily and T. Owens, "Stress around a wellbore," in *Fall meeting of the Society of Petroleum Engineers of AIME*, OnePetro, Denver, Colorado, 1969.

[4] G. Chen, M. E. Chenevert, M. M. Sharma, and M. Yu, "A study of wellbore stability in shales including poroelastic, chemical, and thermal effects," *Journal of Petroleum Science and Engineering*, vol. 38, no. 3-4, pp. 167–176, 2003.

[5] Q. Tao and A. Ghassemi, "Optimization of mud properties for drilling in shale using coupled chemo-poro-thermoelasticity," in *Golden rocks 2006, the 41st US symposium on rock mechanics (USRMS)*, OnePetro, Golden, Colorado, 2006.

[6] A. Ghassemi, Q. Tao, and A. Diek, "Influence of coupled chemo-poro-thermoelastic processes on pore pressure and stress distributions around a wellbore in swelling shale," *Journal of Petroleum Science and Engineering*, vol. 67, no. 1-2, pp. 57–64, 2009.

[7] B. Aadnoy and M. Chenevert, "Stability of highly inclined boreholes," *SPE Drilling Engineering*, vol. 2, no. 4, pp. 364–374, 1987.

[8] B. Haimson and C. Fairhurst, "Initiation and extension of hydraulic fractures in rocks," *Society of Petroleum Engineers Journal*, vol. 7, no. 3, pp. 310–318, 1967.

[9] M. K. Hubbert and D. G. Willis, "Mechanics of hydraulic fracturing," *Transactions of the AIME*, vol. 210, pp. 153–168, 1957.

[10] M. Chenevert, "Shale control with balanced-activity oil-continuous muds," *Journal of Petroleum Technology*, vol. 22, no. 10, pp. 1309–1316, 1970.

[11] H. Rongzun, C. Mian, D. Jingen, W. Kangping, and C. Zhixi, "Study on shale stability of wellbore by mechanics coupling with chemistry method," *Drilling Fluid & Completion Fluid*, vol. 12, pp. 15–21, 1995.

[12] F. K. Mody and A. Hale, "Borehole-stability model to couple the mechanics and chemistry of drilling-fluid/shale interactions," *Journal of Petroleum Technology*, vol. 45, no. 11, pp. 1093–1101, 1993.

[13] E. van Oort, A. Hale, F. Mody, and S. Roy, "Transport in shales and the design of improved water-based shale drilling fluids," *SPE Drilling & Completion*, vol. 11, no. 3, pp. 137–146, 1996.

[14] Y. Lu, C. Mian, J. Yan, T. Xueqing, W. Wu, and L. Xuquan, "Experimental study of strength properties of deep mudstone underdrilling fluid soaking," *Chinese Journal of Rock Mechanics and Engineering*, vol. 31, pp. 1399–1405, 2012.

[15] L. Xiangjun, X. Jian, and L. Liang, "Hydration experiment of hard brittle shale of the Longmaxi formation," *Journal of Southwest Petroleum University (Science & Technology Edition)*, vol. 38, pp. 178–186, 2016.

[16] J. Changgui, C. Junhai, Y. Guo, C. Yang, J. Xu, and L. Wang, "Research on mechanical behaviors and failure modes of layer shale," *Rock and Soil Mechanics*, vol. 34, pp. 57–61, 2013.

[17] J. Jaeger, "Shear failure of anistropic rocks," *Geological Magazine*, vol. 97, no. 1, pp. 65–72, 1960.

[18] T. Ma and C. Ping, "Analysis of wellbore stability for horizontal wells in stratification shale," *Journal of Southwest Petroleum University (Science & Technology Edition)*, vol. 36, pp. 97–104, 2014.

[19] M. Meng, S. Baldino, S. Miska, and N. Takach, "Wellbore stability in naturally fractured formations featuring dual-porosity/single-permeability and finite radial fluid discharge," *Journal of Petroleum Science and Engineering*, vol. 174, pp. 790–803, 2019.

[20] X. Yan, L. You, Y. Kang, X. Li, C. Xu, and J. She, "Impact of drilling fluids on friction coefficient of brittle gas shale," *International Journal of Rock Mechanics and Mining Sciences*, vol. 106, pp. 144–152, 2018.

[21] A. Dominijanni, E. Fratalocchi, N. Guarena, M. Manassero, and F. Mazzieri, "Critical issues in the determination of the bentonite cation exchange capacity," *Géotechnique Letters*, vol. 9, no. 3, pp. 205–210, 2019.

[22] C. Wenke, *Study of Mechanical-Chemical-Thermal Coupling Effect on Wellbore Stability in Anisotropic Shale Formation*, China University of Petroleum (Beijing), Beijing, China, 2017, (Doctoral Dissertation).

[23] Y. Wang, X. Liu, Y. Zeng, and X. Guang, "Research on integrated classification method of claystones and shales," *Drilling Fluid & Completion Fluid*, vol. 31, pp. 82–85, 2014.

[24] A. Diaz Perez, *Chemoporoelastic solution of transversely isotropic saturated porous media*, University of Oklohama, Oklohama, Norman, 2004, (Doctoral Dissertation).

[25] A. Ghassemi and A. Diek, "Effects of ion transfer on stress and pore pressure distributions around a borehole in shale," in *DC rocks 2001, the 38th US symposium on rock mechanics (USRMS)*, OnePetro, Washington, D.C, 2001.

[26] E. Detournay and A.-D. Cheng, "Poroelastic response of a borehole in a non-hydrostatic stress field," *International Journal of Rock Mechanics and Mining Sciences & Geomechanics Abstracts*, vol. 25, no. 3, pp. 171–182, 1988.

[27] P. Shengyu, "Research progress of semi-permeable membrane formation based on drilling fluid-shale interface," *Inner Mongolia Petrochemical Industry*, vol. 39, pp. 109–112, 2013.

[28] A. Diek, L. White, J.-C. Roegiers, K. Bartko, and F. Chang, "A fully coupled thermoporoelastic model for drilling in chemically active formations," in *45th US Rock Mechanics/Geomechanics Symposium*, OnePetro, San Francisco, California, 2011.